

Figure 4.1. The four levels of geometry. The levels of geometry can be defined through what is seen by an observer whose eye gets closer and closer to a point in space. We examine the shape of space with a telescope of variable magnification, centered on a chosen point x . At magnification 1, the field of view includes the global geometry of space, whose shape could be extremely complicated (level 1). When the magnification grows, a smaller portion of the space appears in the field of view, which looks like a more or less curved disc; this is the space of macroscopic geometry (level 2). When the magnification grows even more, the disc is reduced to a smaller and smaller neighborhood of the point, its curvature becomes imperceptible and it seems flat; this is the space of local geometry (level 3). At nearly infinite magnification, we see the intimate microscopic structure of space, which may once again become very complicated (level 4). In the column on the right, I have indicated the various theories of fundamental physics that, at the present time, seem to be in the best position to describe correctly the corresponding level of magnification.

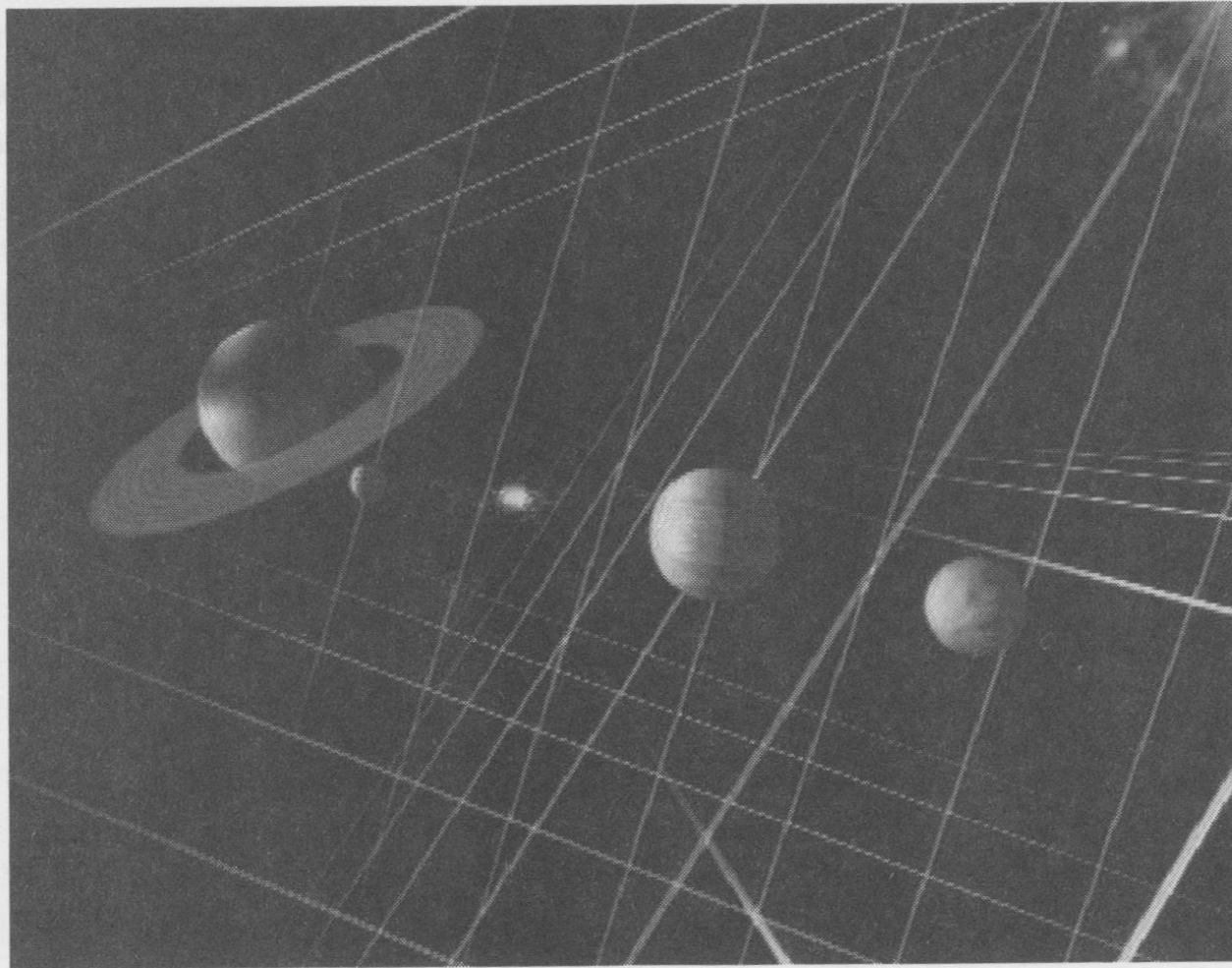


Figure 5.1. The Newtonian Universe. This view of Newtonian cosmic space allows one to visualize the structure of infinite Euclidean space, woven through with light rays following rectilinear trajectories. Planets, stars, and galaxies move along orbits curved by the universal attractive force of gravity. (Image from the film *Infiniment Courbe*, © Laure Delesalle.)

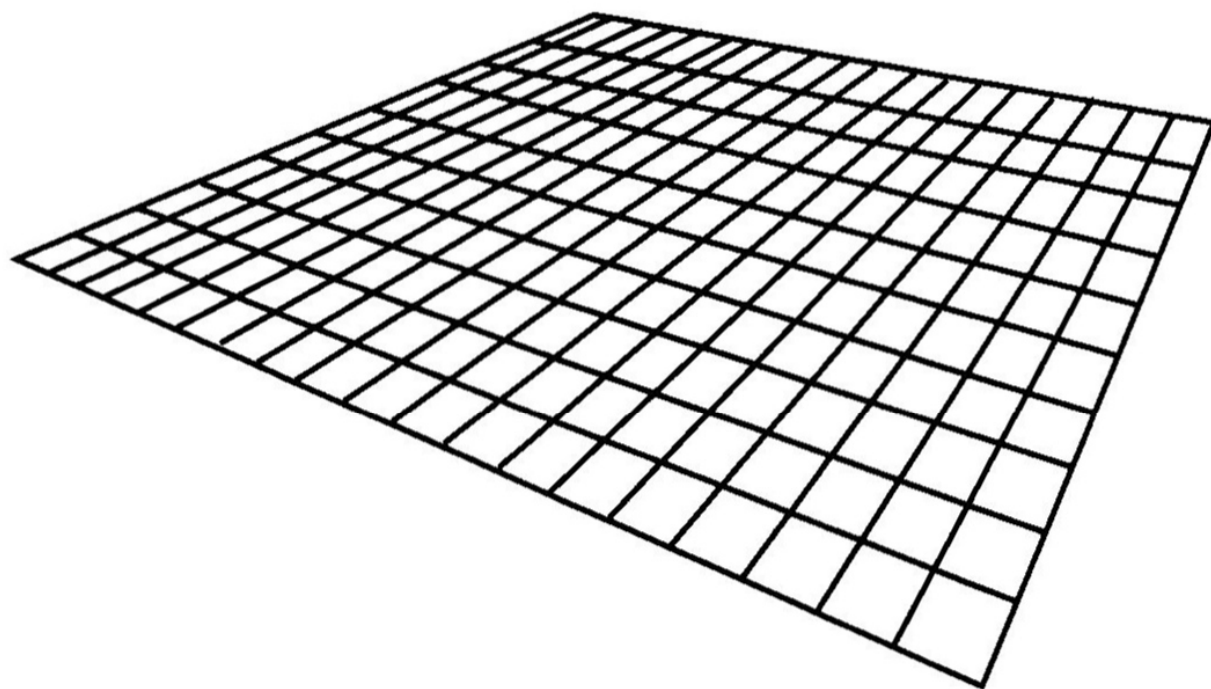


Figure 5.3. Flat elastic fabric. In the absence of mass, which is to say the absence of gravity, the fabric of space-time has no curvature. The trajectories of light rays trace out a rectilinear grid, which defines the Euclidean geometry of space.

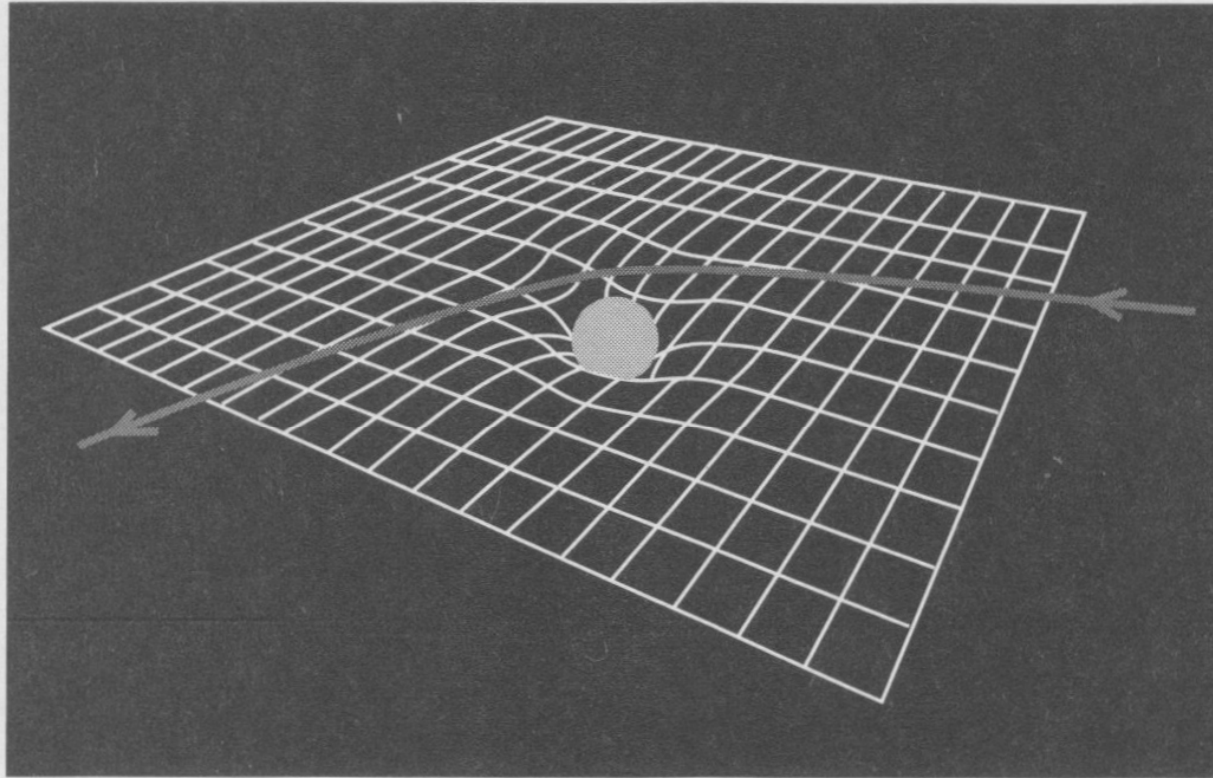
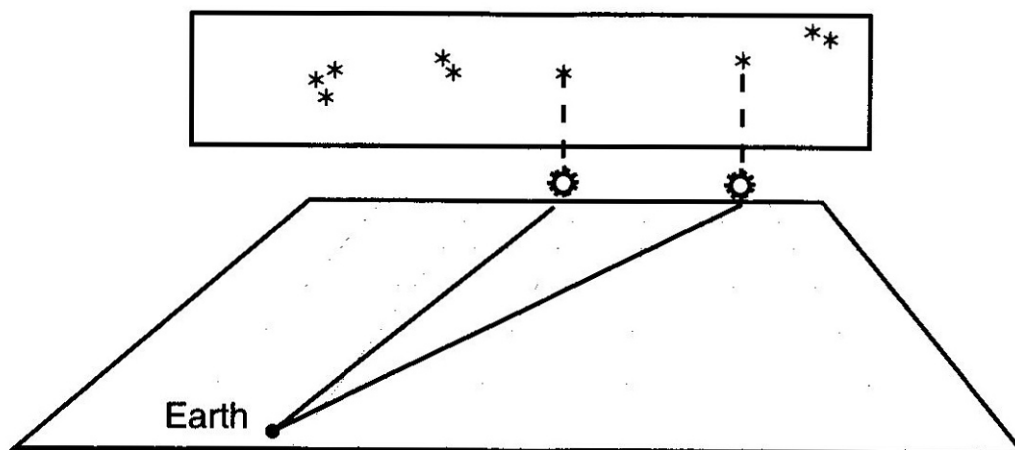
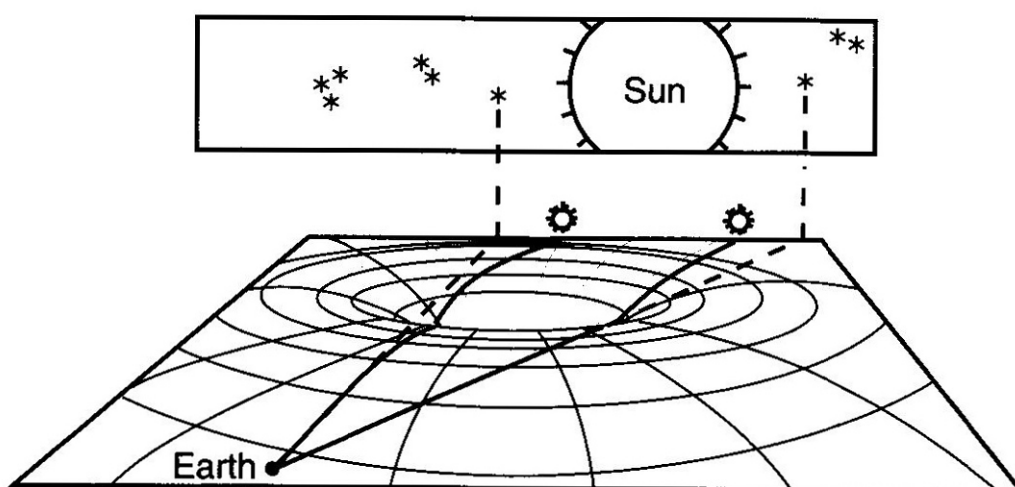


Figure 5.4. Curved elastic fabric. In the relativistic framework, gravity is an illusory force created by the curvature of the Universe. A massive star like the Sun imprints a dent into the elastic fabric of space-time. The trajectories of bodies naturally follow the curvature of the fabric.



(a) real position of the stars in the absence of the Sun



(b) apparent position of the stars during an eclipse of the Sun

Figure 5.5. The deflection of light rays by the Sun. When the Sun is placed in front of a distant field of stars (visible only during a sufficiently long total eclipse), it curves the space-time in its vicinity and deflects the light rays coming from behind it. The apparent direction of the stars (b) is shifted with respect to their real position (a).

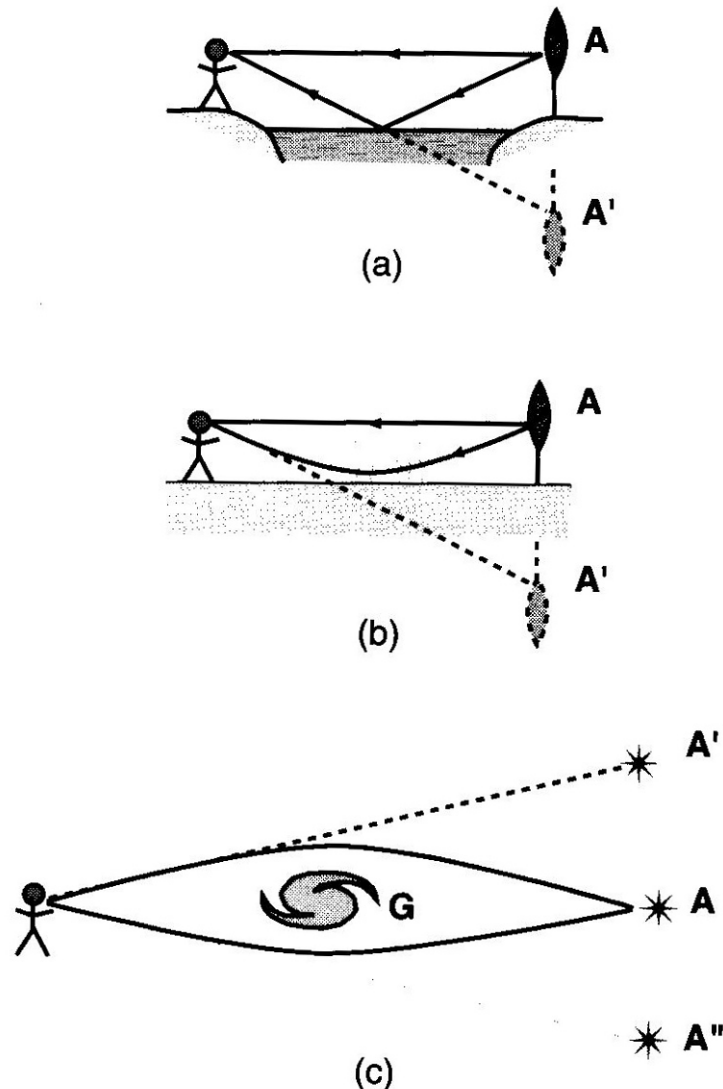


Figure 6.1. The principle behind mirages. (a) Light reflection from an aquatic surface situated between the observer and the object A causes two light rays issuing from A to meet once again; there is a doubling of the image. (b) In a terrestrial mirage, the light rays issuing from A are refracted and deflected while crossing overheated layers of air near the ground. Once again, there is a multiplication of images. (c) In a gravitational mirage, a massive body G situated between the observer and the luminous source A deflects, deforms, and multiplies the images of A .

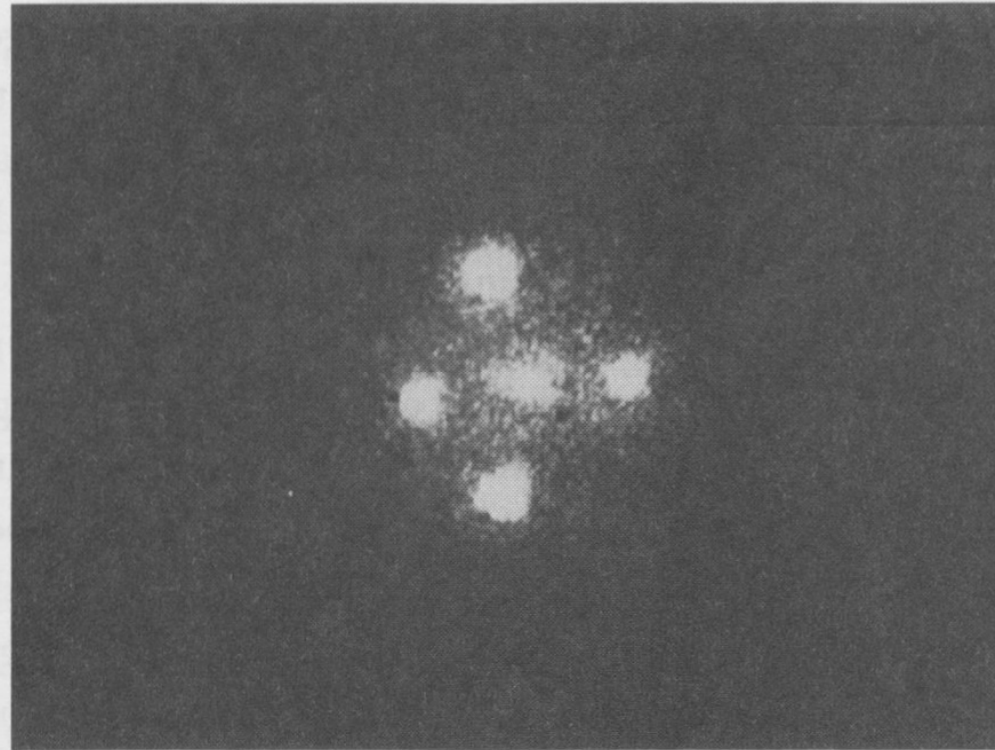


Figure 6.2. The Einstein Cross. This gravitational mirage was photographed by the Hubble space telescope. Four copies of a quasar, situated eight billion light years away, are observed because of a lens galaxy (at the center) which is twenty times closer. (Image from STScI/NASA.)

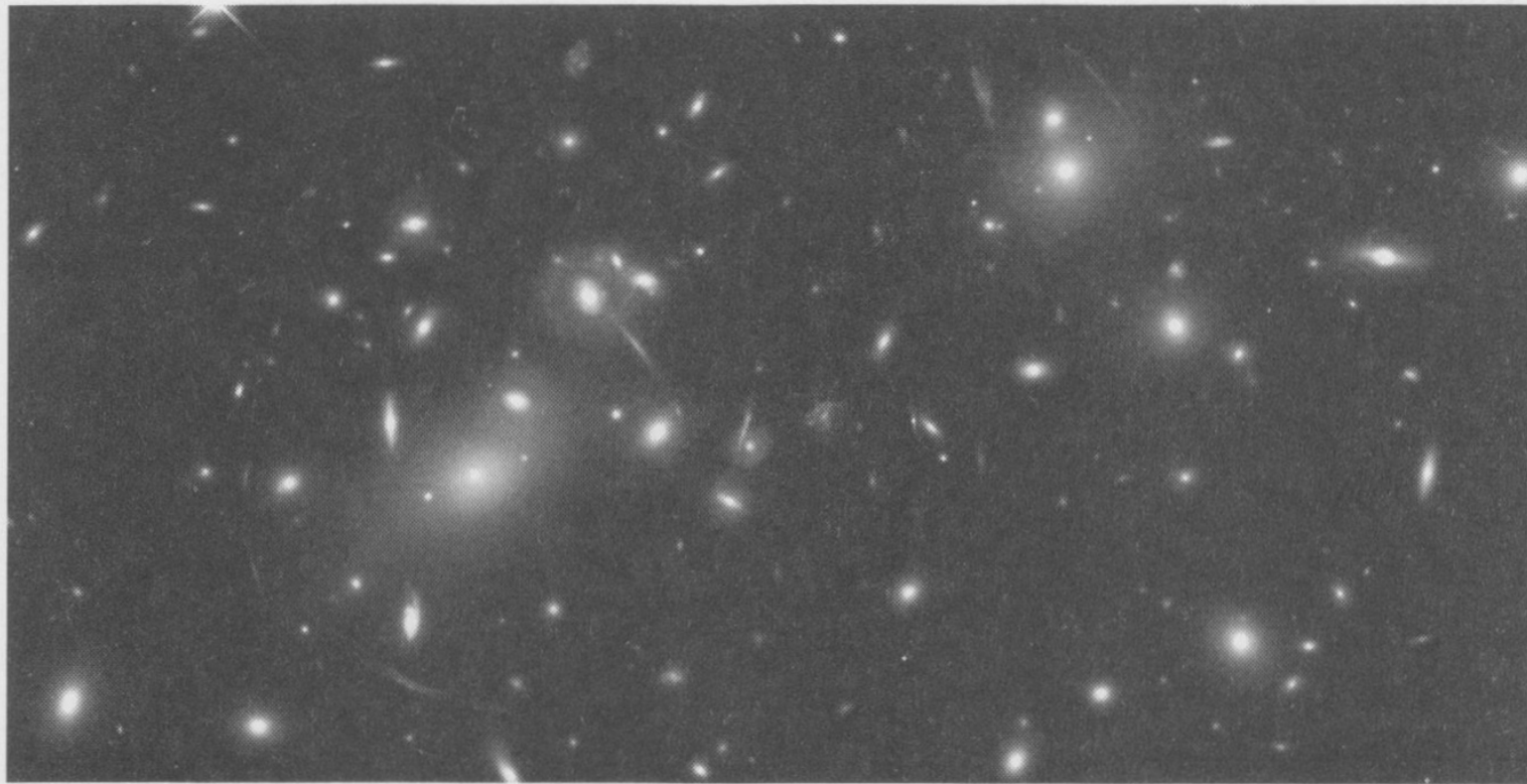


Figure 6.3. Gravitational arcs. The most spectacular mirages lead to the formation of luminous arcs. These arcs are the highly distorted images of distant galaxies, situated in the background of the galaxy cluster Abell 2218 (in yellow in the photograph). The gravitational effects of the cluster bend the light rays and distort the images, ultimately giving the images their characteristic arc shape. (See Plate I. Image from STScI/NASA.)

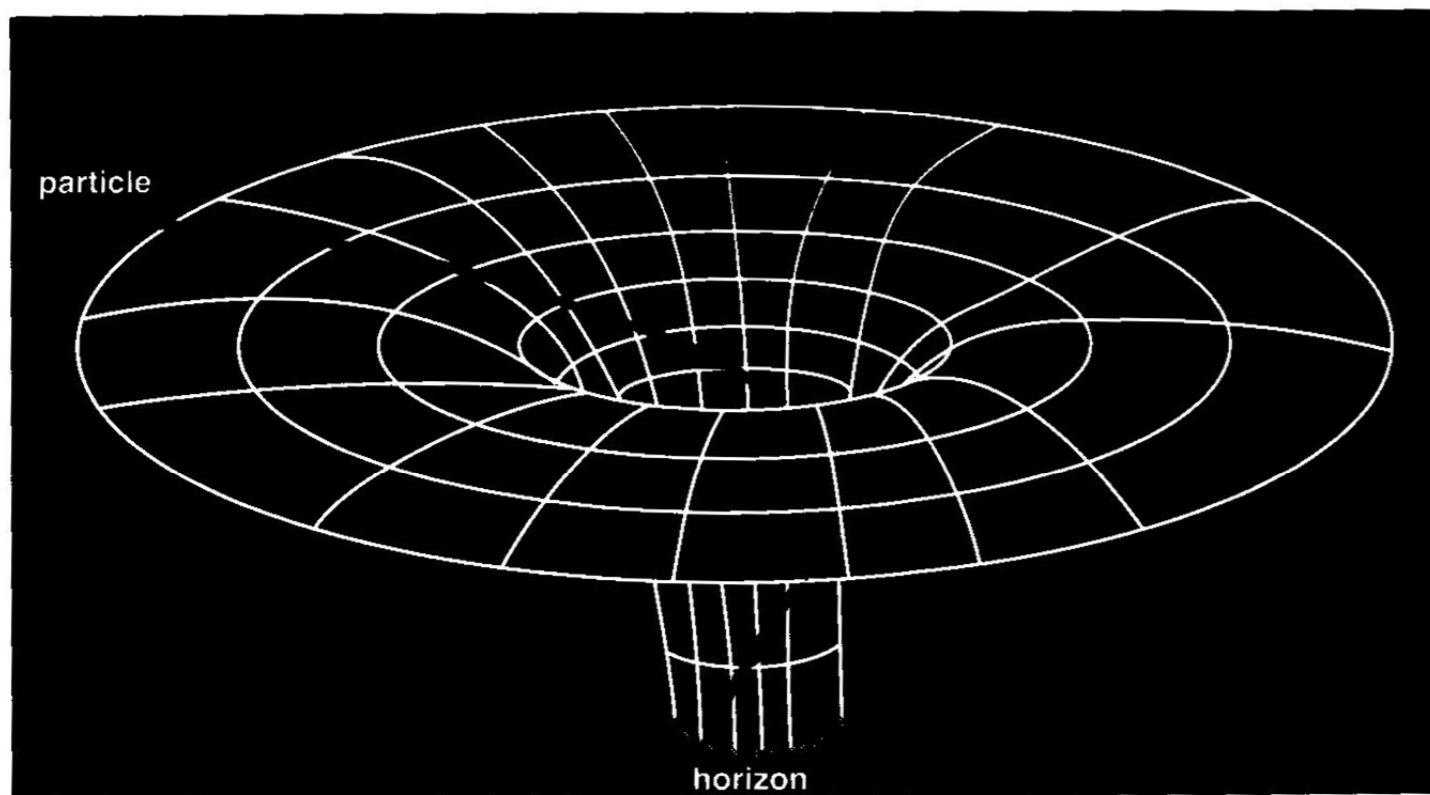


Figure 7.1. The well of the black hole. The black hole forms a gravitational well in the elastic fabric of space-time that is so deep that every particle and every light ray that crosses its edge is captured. The surface of the black hole, called the event horizon, has no material consistency: it is a purely geometric border around a zone of no return.

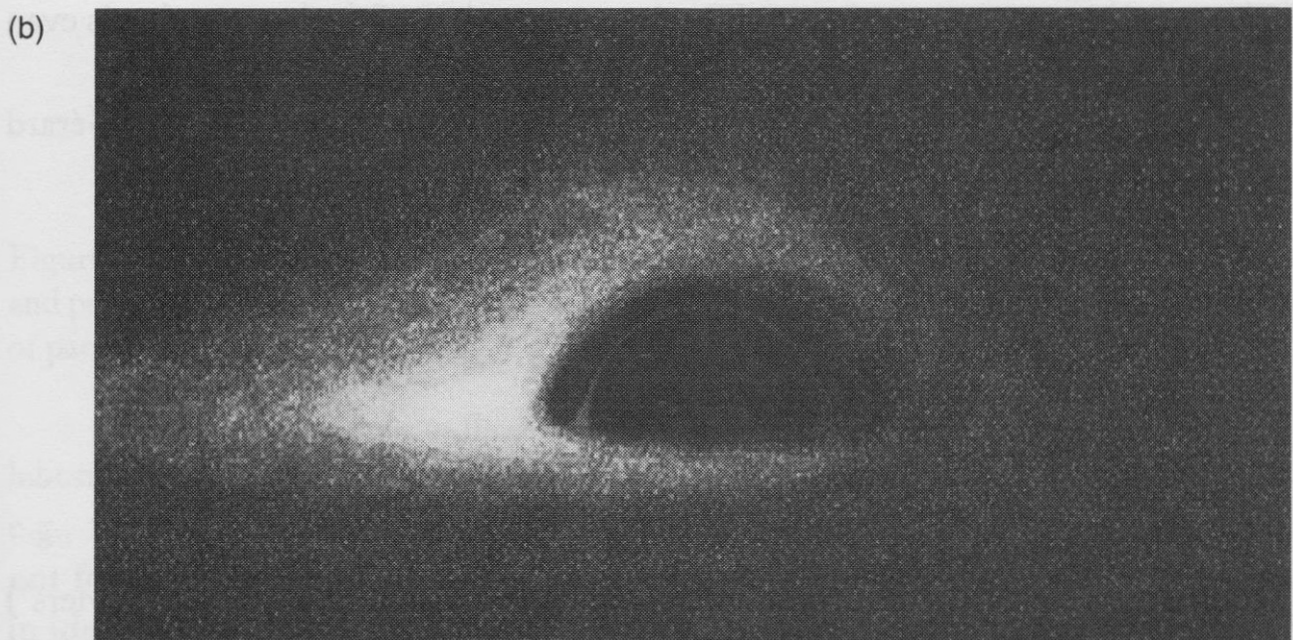
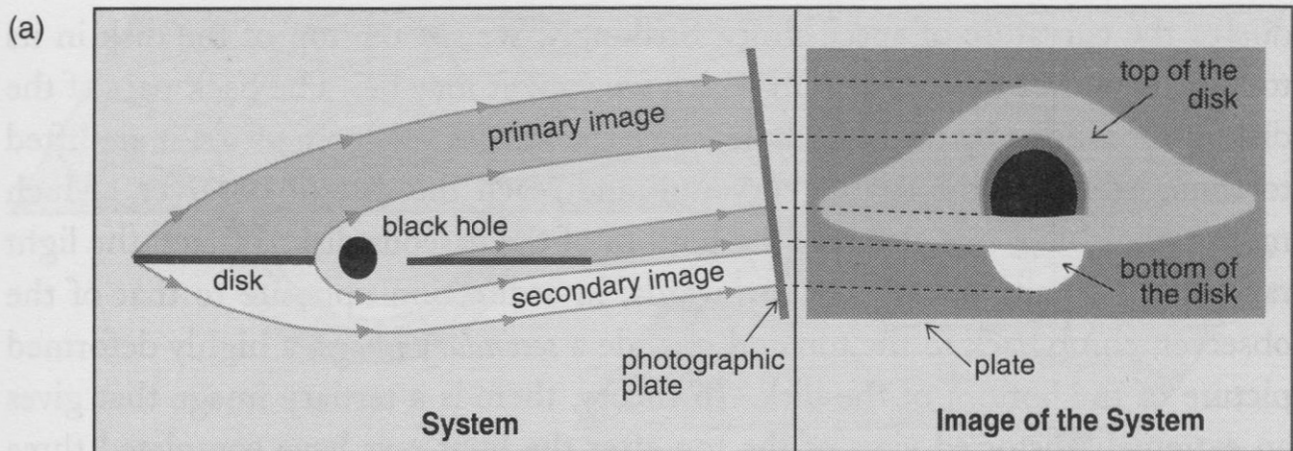


Figure 7.2. The black hole photographed. (a) A black hole, surrounded by a thin disk of gas and viewed from very far away in a direction weakly inclined with respect to the plane of the disk. General relativity allows the calculation of the deflection of light rays due to the strong curvature of the space-time in the vicinity of the black hole; it allows one to see all of the top of the disk and part of the bottom. (b) By accounting also for the physical properties of the gaseous disk, in particular rotation (which gives the left right asymmetry of the light flux), temperature, and emissivity, this simulation of the photographic appearance of a black hole surrounded by a disk of luminous gas was completed on the computer at the Meudon observatory in France in 1979.

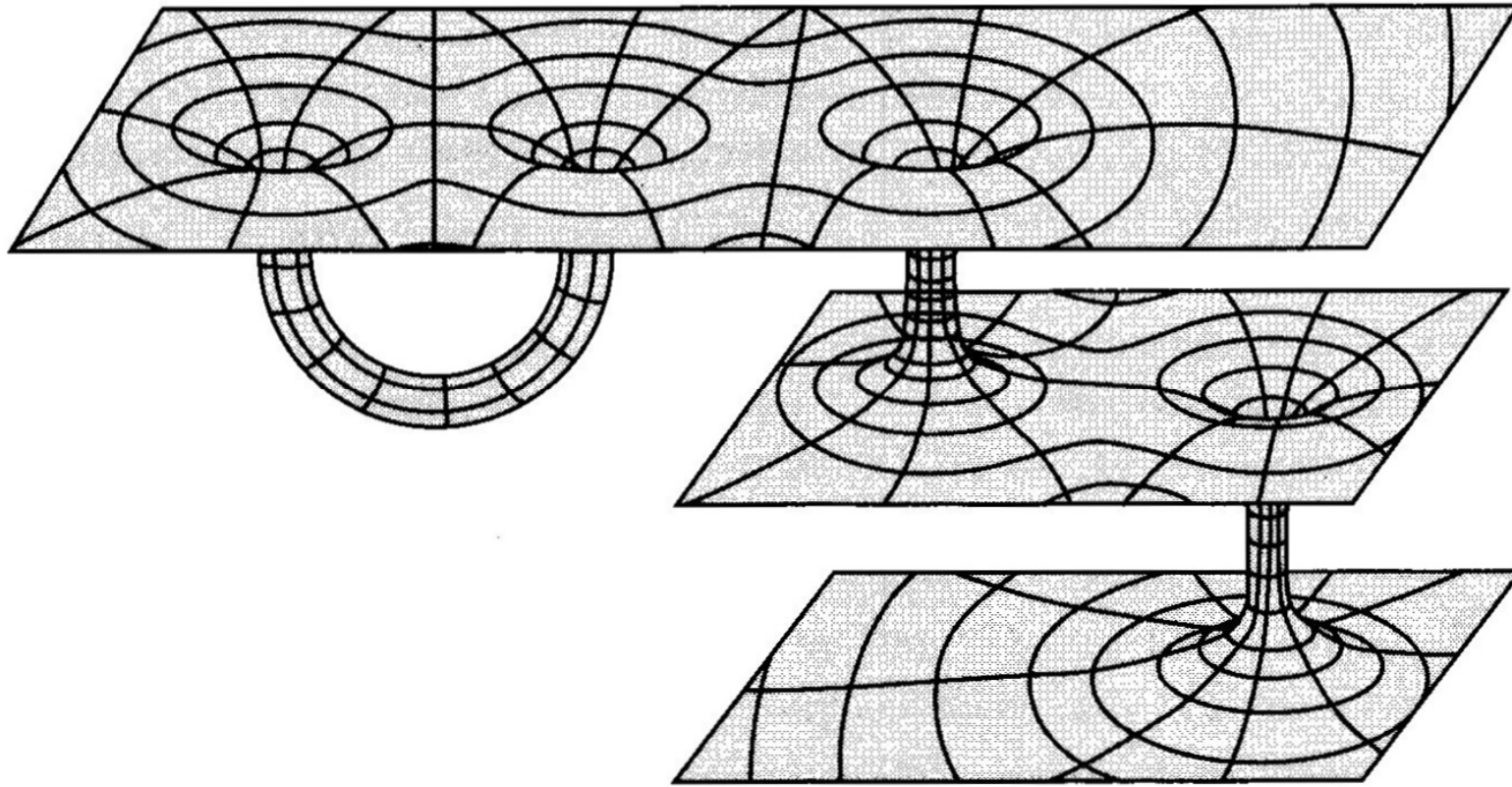


Figure 7.3. Wormholes. Wormholes could interconnect distant regions of the Universe and permit interstellar voyages in space and time. They could also connect an infinite series of parallel universes.

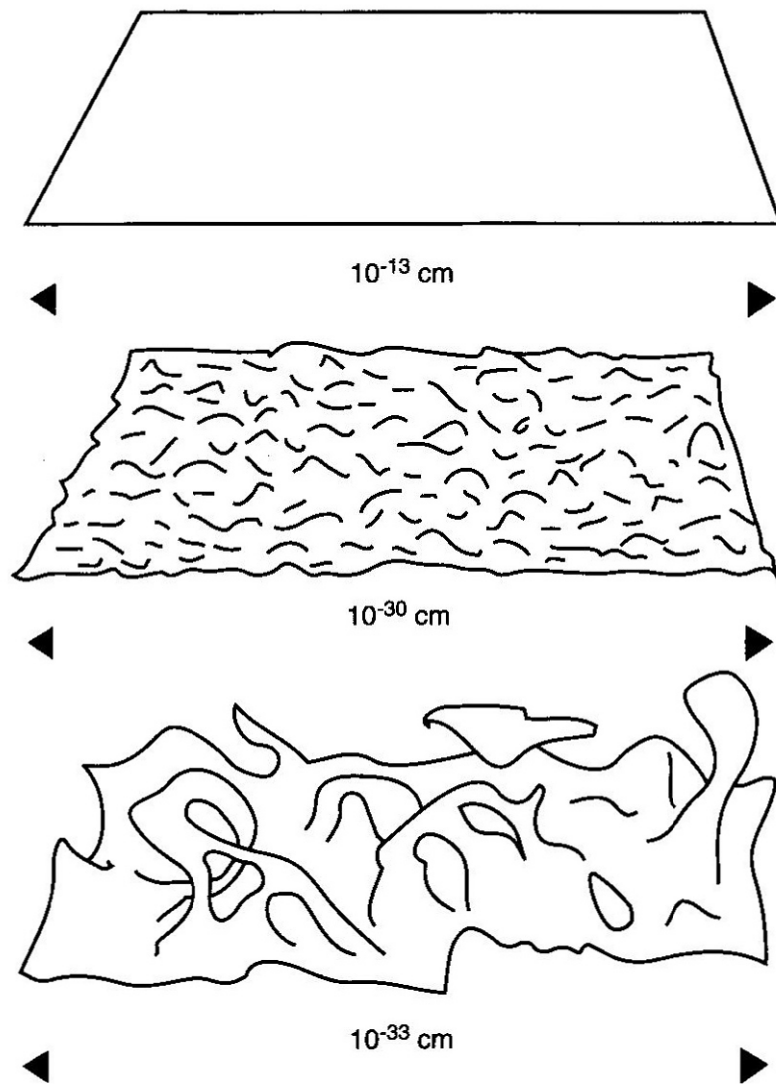


Figure 8.1. Space-time foam. At the microscopic level, space-time is well described by a smooth continuum, deprived of roughness like the surface of the ocean seen from high altitude. Approaching the quantum level, the fluctuations of space-time geometry should become perceptible, like waves on the ocean. At the truly quantum level (10^{-33} cm), the fluctuations would completely dominate the geometry, which would then become extremely tormented, in perpetual transformation like foam on the waves.

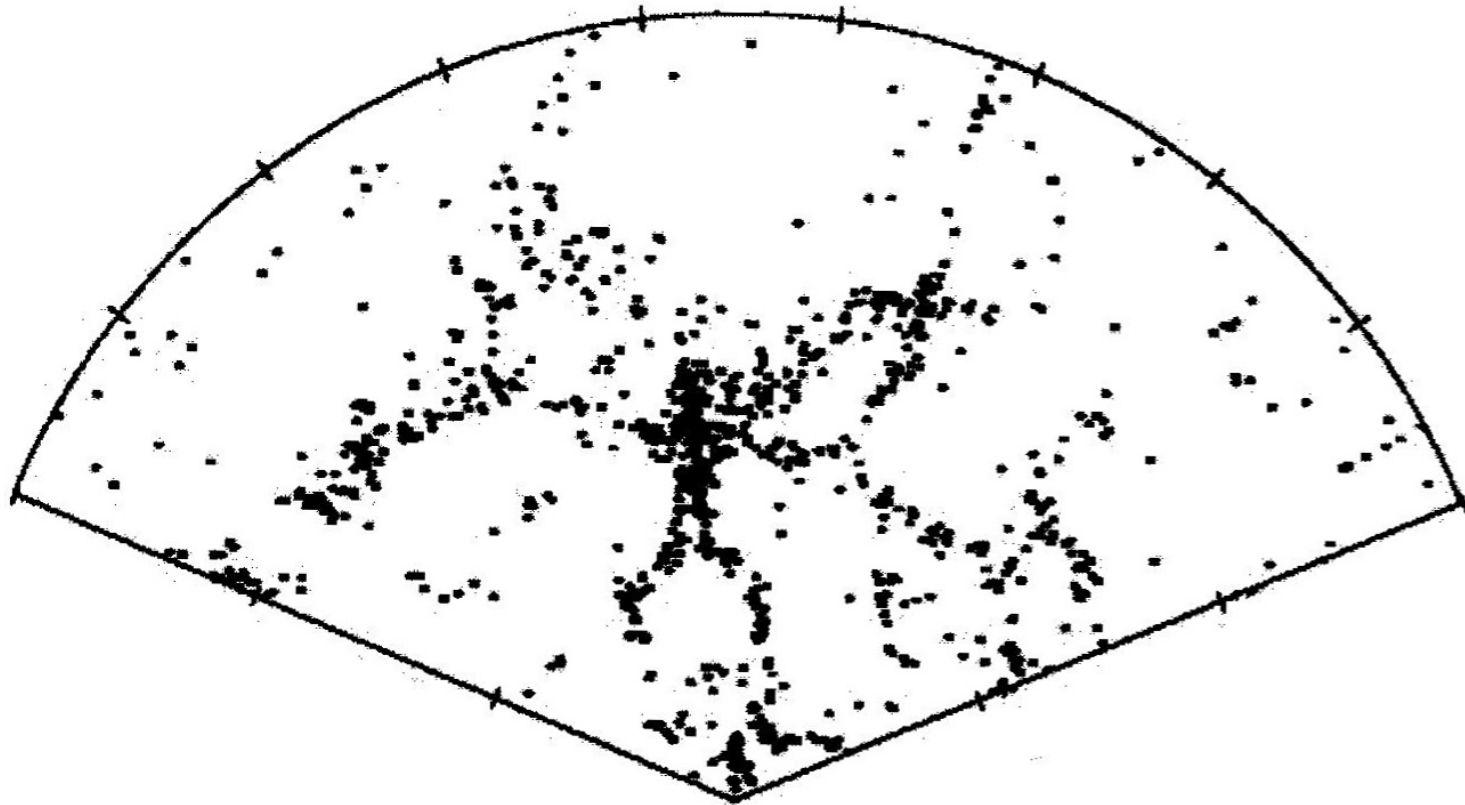


Figure 9.1. The cosmic Great Wall. Galaxies are grouped in clusters, and galaxy clusters are assembled into larger structures, the superclusters. The slice of space represented here includes more than a thousand galaxies, grouped in filaments organized around empty bubbles. A strange structure, in the form of a stick figure viewed face on, with legs and arms spread out, stands out 300 million light years from Earth. The arms of the stick figure stretch out for more than 500 million light years, but measure no more than 15 million light years in thickness—from whence the name “Great Wall.” (Image adapted from M. Geller et al.)

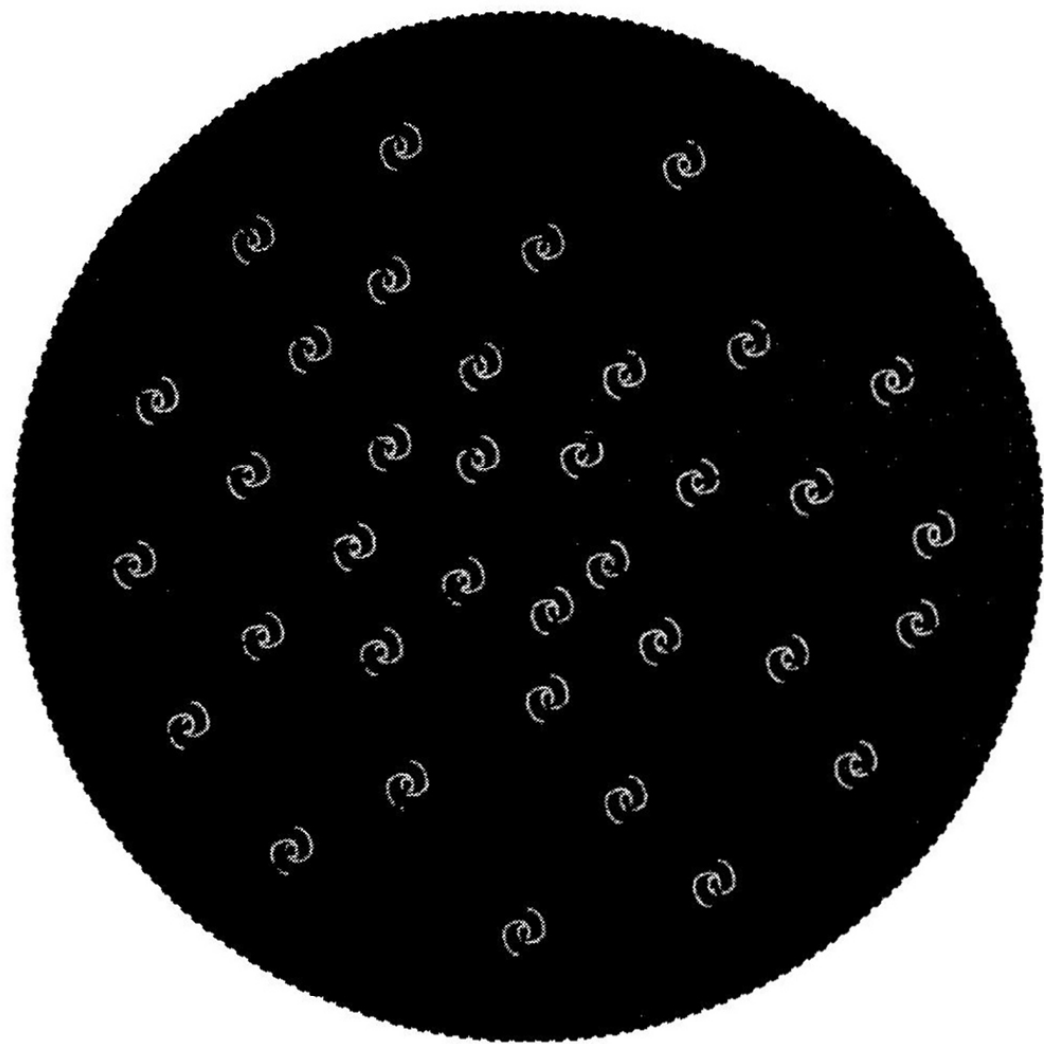


Figure 9.3. Does the recession of other galaxies imply an explosion? Around us, we observe that other galaxies systematically move away at radial velocities that are larger (as shown by the arrows), the farther away they are. Does this mean that we are at the center of a great explosion, as the figure suggests? No, because by virtue of the cosmological principle, at every point in space the same type of observation could be made. Space expands at every one of its points.

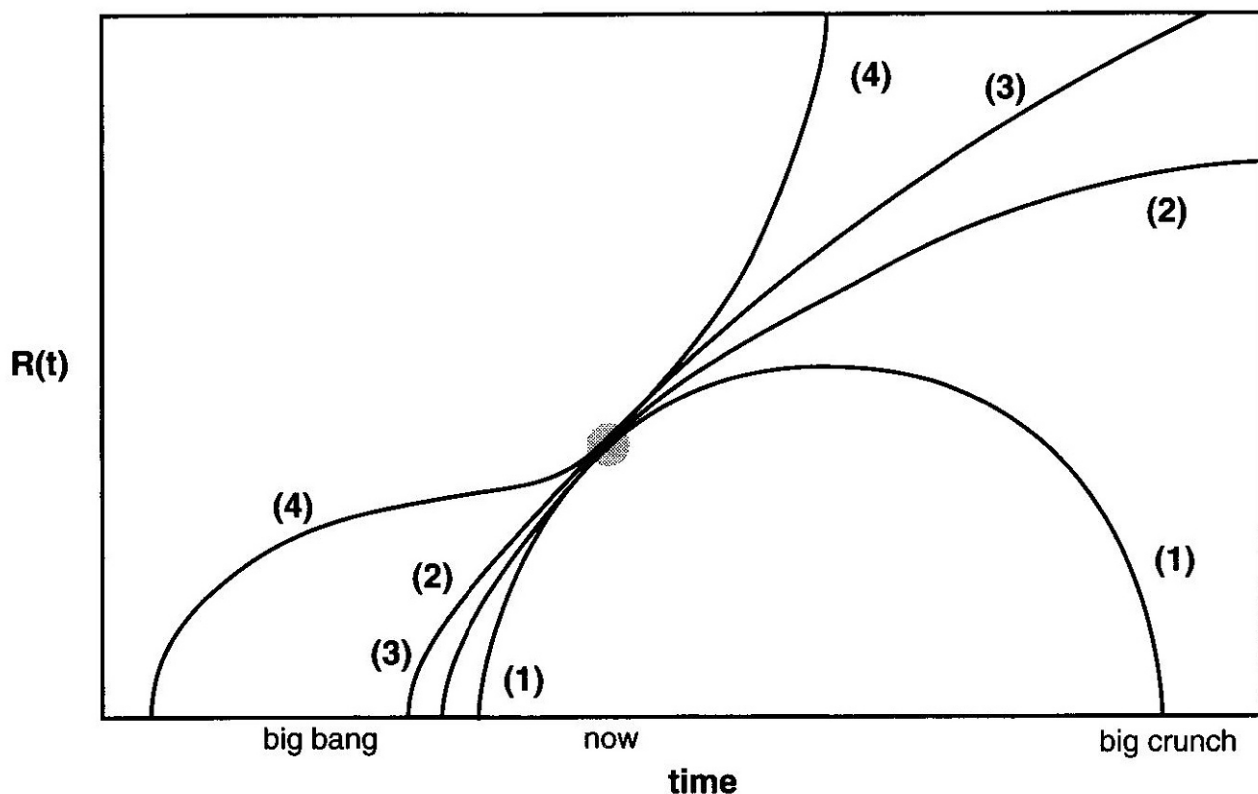
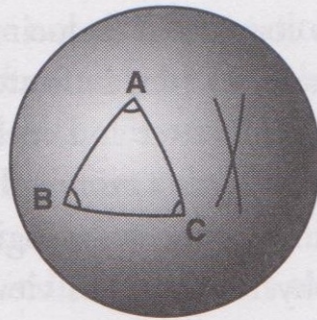
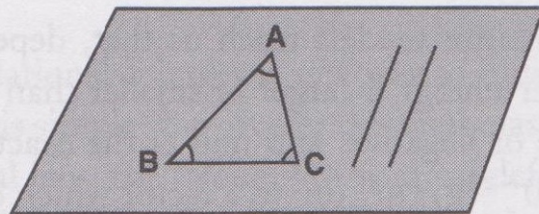


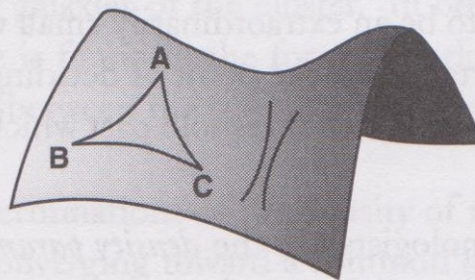
Figure 9.5. Big-bang models. Homogeneous and isotropic cosmological models, called Friedmann-Lemaître models, are classified by their curvature and their dynamics. Their essential characteristic is that they are solutions where space varies over the course of time. We represent (along the y -axis) a spatial scale factor, that is to say, the distance between two arbitrary sufficiently distant points, whose separation one measures over the course of time (the x -axis). The viable models of the big bang are the closed (1) and open (2) Friedmann-Lemaître models, the Einstein-de Sitter model (3)—a particular case with strictly zero curvature—and the Lemaître model of accelerated expansion, (4). The small circle represents the present epoch. To determine on which branch we really are, and therefore to extrapolate the ultimate destiny of the universe and its distant past, we must determine the density and the nature of cosmic energy. Present measurements tend to favor the model of accelerated expansion, (4).



$$A + B + C > 180^\circ$$



$$A + B + C = 180^\circ$$



$$A + B + C < 180^\circ$$

Figure 10.1. Three types of curved surfaces. The surface of the sphere has positive curvature, the plane has zero curvature, and a horse saddle has negative curvature. On the sphere, the sum of the angles in a triangle is greater than 180 degrees; in the plane, it is exactly equal to 180 degrees; and on the saddle, it is less than 180 degrees. Three-dimensional spaces can be curved just like surfaces, but in a more complicated fashion. In principle, one could detect the curvature of the Universe by measuring the angles formed by a gigantic cosmic triangle.


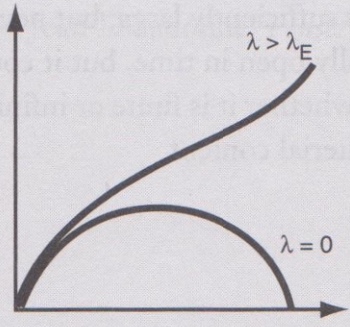
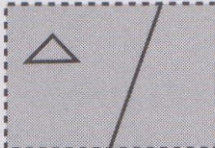
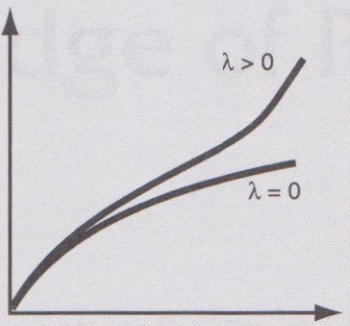

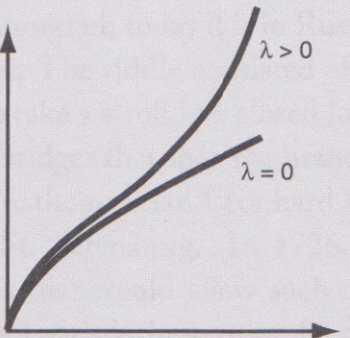
curvature	topology	dynamics	fate
$K > 0$  spherical	finite		Open if λ is large closed
$K = 0$  Euclidean	finite or infinite		open
$K < 0$  hyperbolic	finite or infinite		open

Figure 11.1. Open or closed? Contrary to a currently widespread opinion, the curvature of space dictates neither the temporal evolution of the Universe (unless the cosmological constant is zero), nor the finite or infinite character of space (unless the topology is simply connected). The table summarizes the different possible cases for big-bang models. The first column shows the sign of the spatial curvature, the second the finite or infinite character of space, the third the temporal behavior of the scale factor, the fourth the open or closed character of the model.

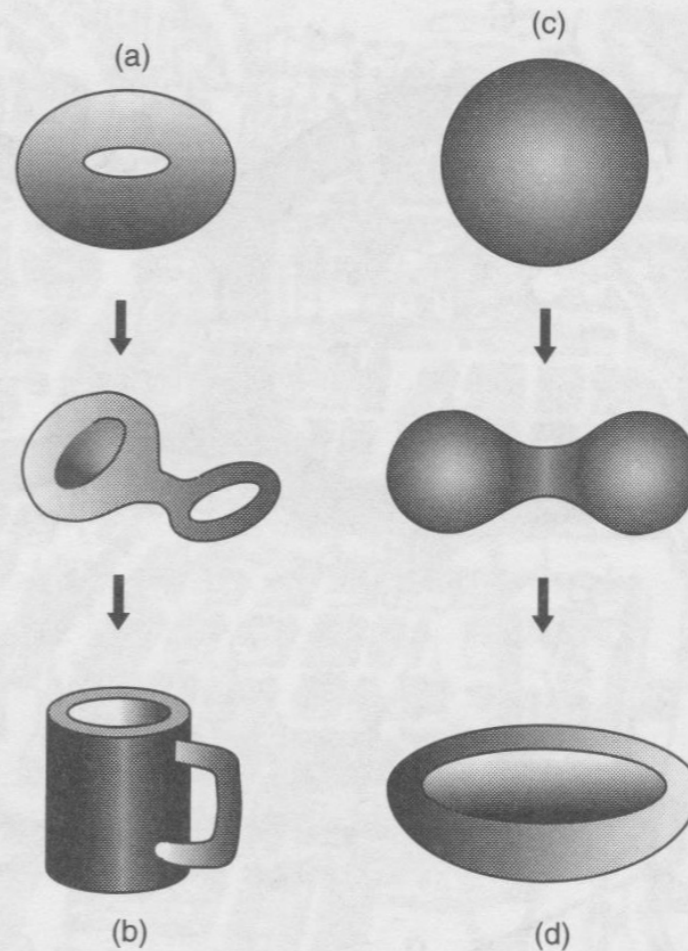


Figure 12.3. Continuous deformations. Let us imagine that the surface of a ring (a) is made of rubber, and that one can easily stretch it without tearing it. We deform part of the surface to form a bump, then transform this bump into a sort of sac which is larger than the original ring. The ring has become a coffee cup with a handle (b)! It is impossible, though, with any continuous deformation whatsoever, to obtain a bowl (d). The surface of a sphere (c), however, can do the job.

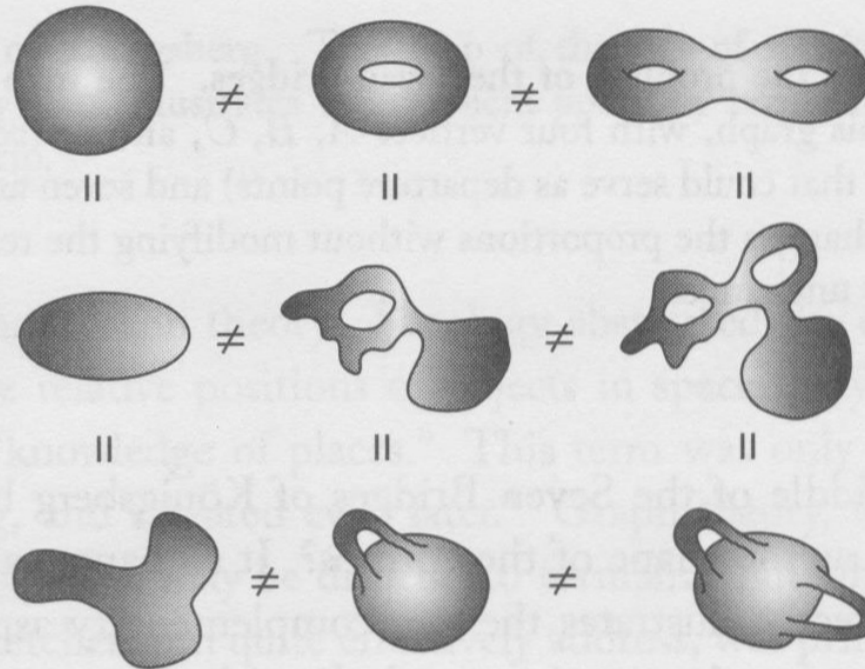


Figure 12.4. Sphere and tori. In the case of two-dimensional spaces, that is to say surfaces, the sphere has the same topology as any closed surface without a hole. Tori with one or more holes have different topology; they can be continuously deformed into spheres equipped with handles.

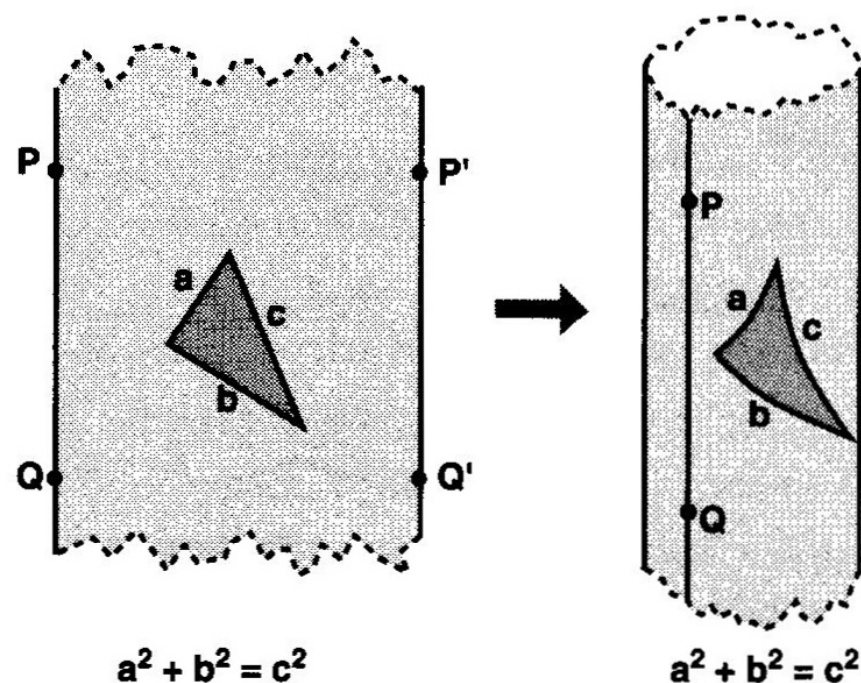


Figure 13.2. Constructing the cylinder. After having cut a strip of paper from the plane, we glue the opposite edges, which is the same as identifying the points P with P' and Q with Q' . The resulting surface is a cylinder. To us this seems to have curvature. In reality, the cylinder is flat: if a square triangle is traced, the Pythagorean Theorem remains perfectly valid.

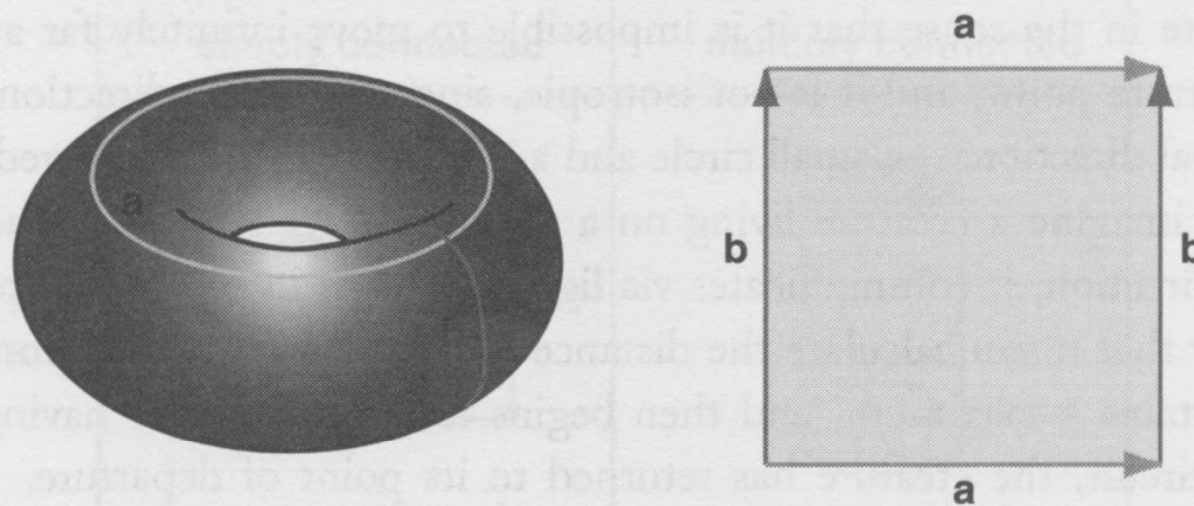


Figure 13.4. Constructing the flat torus. From the topological point of view, a flat torus is obtained by gluing the opposite sides of a rectangle. Inversely, if we cut the torus (left) along the two lines a and b , we can unroll it in a rectangle (right).

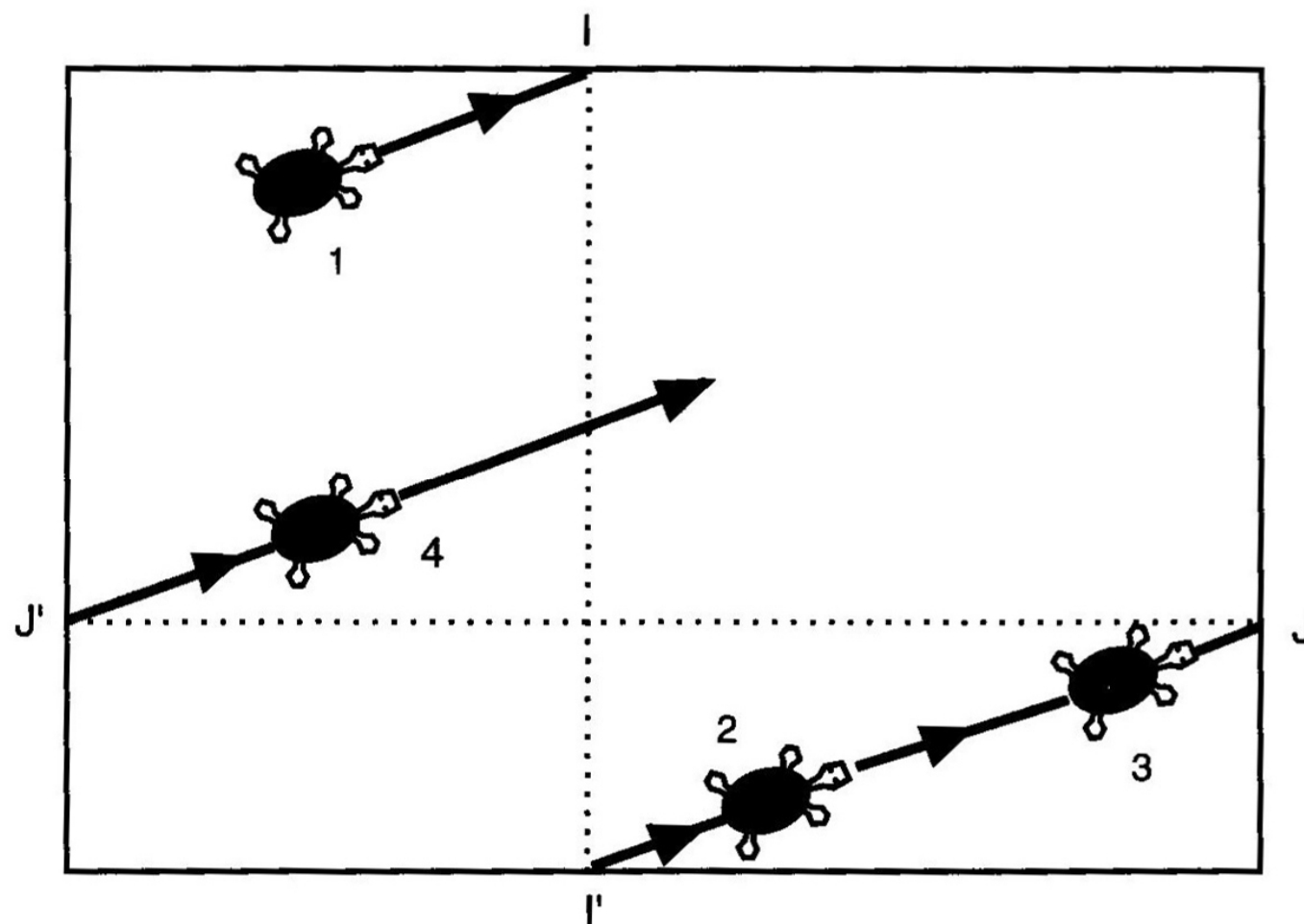


Figure 13.6. A trip on the torus. As in those video games in which the characters who leave on one side reenter on the opposite side, the turtle crosses the upper edge of the rectangle at I and reappears on the lower edge, at the equivalent point I' . Following his path in a straight line, he reaches the right edge at J , reappears at J' , and so on. The torus is thus equivalent to a rectangle whose opposite edges are identified two by two.

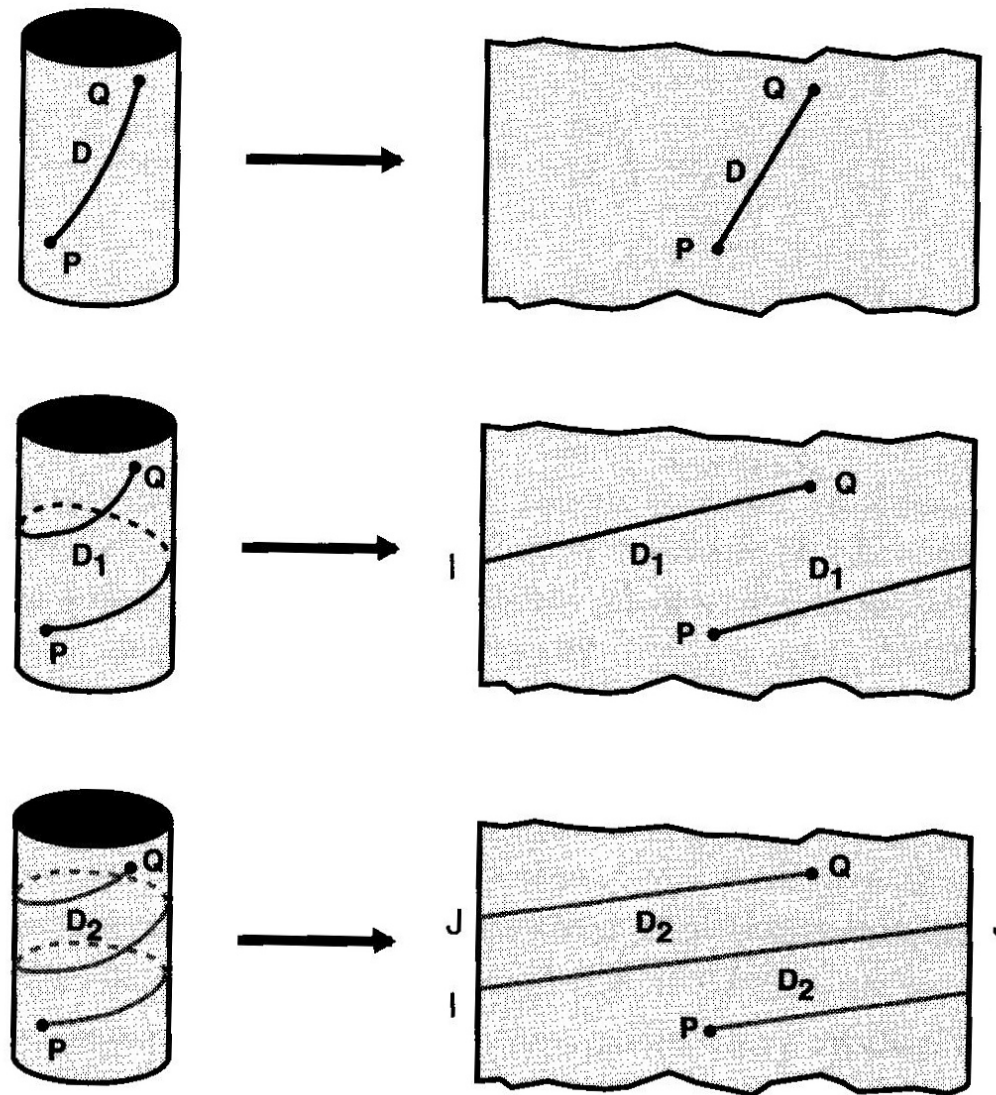


Figure 13.3. Straight lines on the cylinder. Straight lines on a cylinder are helices with constant spacing. Two arbitrary points P and Q are connected by an infinite number of helices D making $0, 1, 2, \dots$ turns around the cylinder. If we unroll the cylinder in the plane, all of these helices indeed roll out in the shape of straight lines.

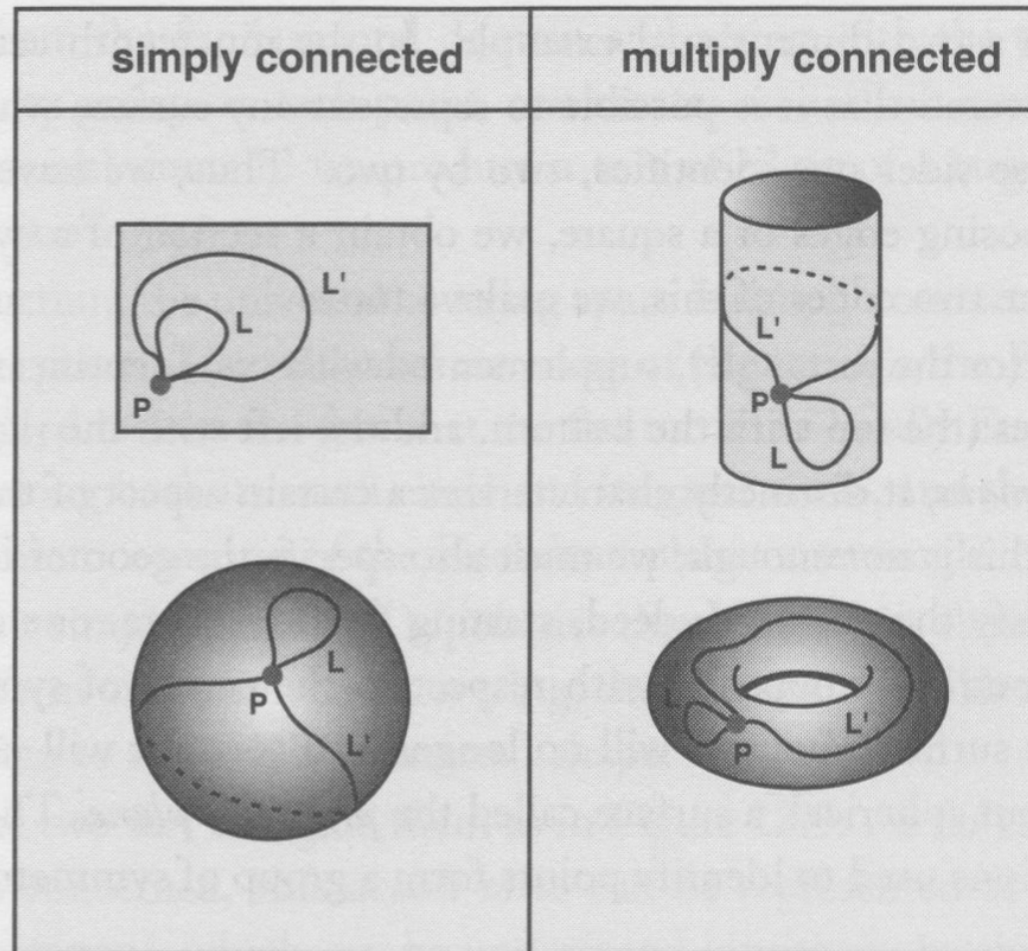


Figure 13.7. Laces and connectivity. In a plane or on a sphere, all laces can be indefinitely tightened, without obstacle. These spaces are simply connected. On a cylinder or a torus, some laces can be tightened, others not. These spaces are multiply connected.

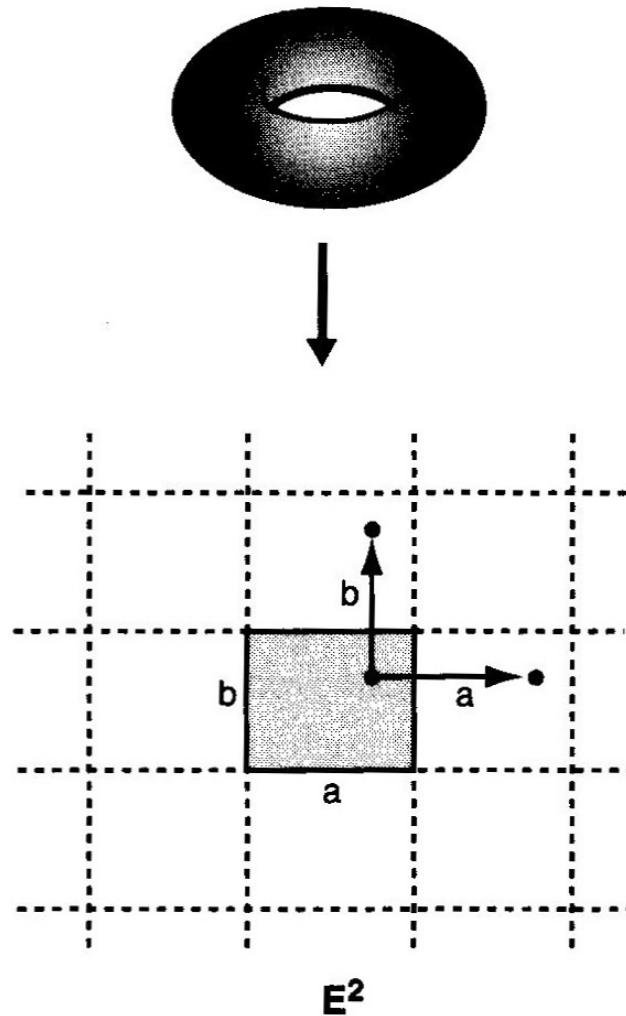


Figure 13.8. The universal covering. The fundamental domain for a torus is a rectangle, and the holonomies are translations by distances equal to the sides of the rectangle. By acting with the holonomies on each point in the fundamental domain, and by repeating the process again and again, one creates the universal covering space—here the Euclidean plane E^2 .

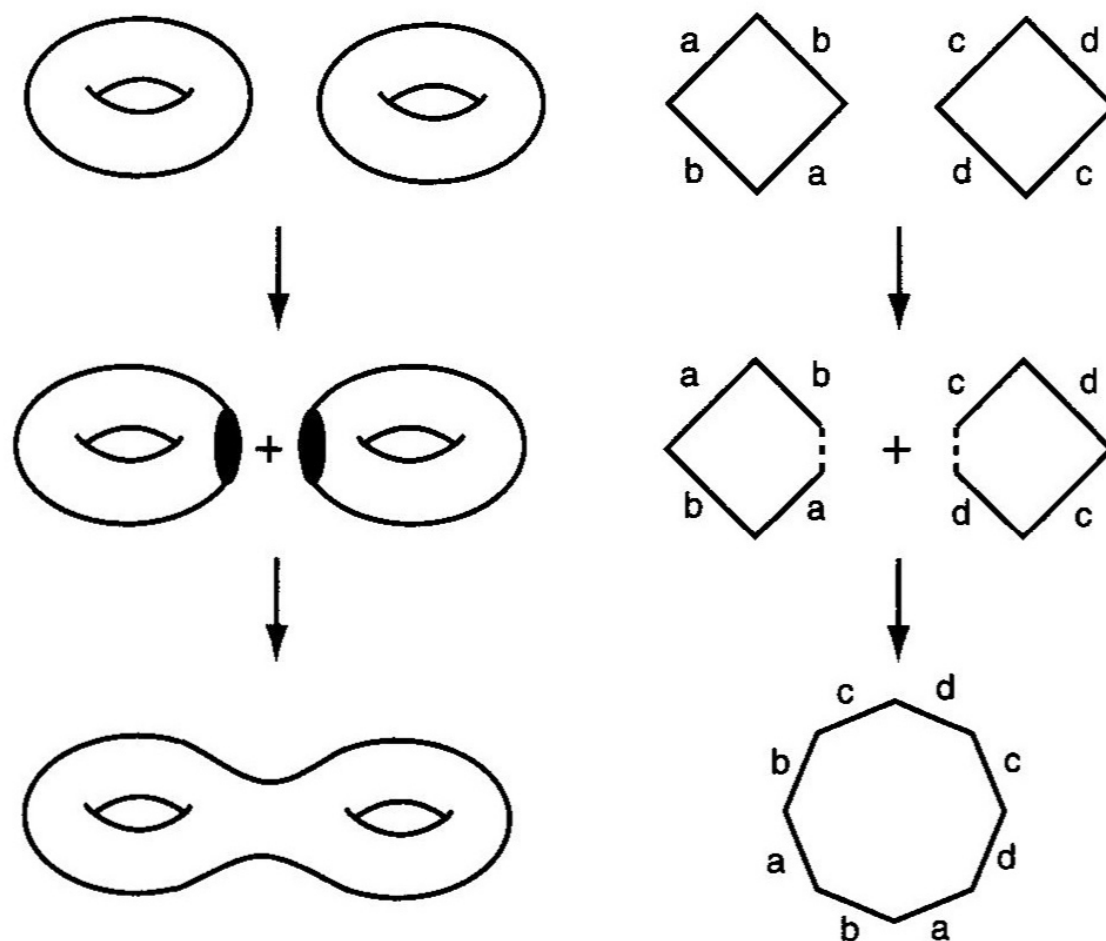


Figure 13.9. Connected sum of tori. The left column shows disks being removed from each of two tori; the edges of the holes are then glued to form a double torus. The right column shows the same operation starting from fundamental domains. The double torus can be represented by an octagon whose edges have been identified two by two in a certain way.

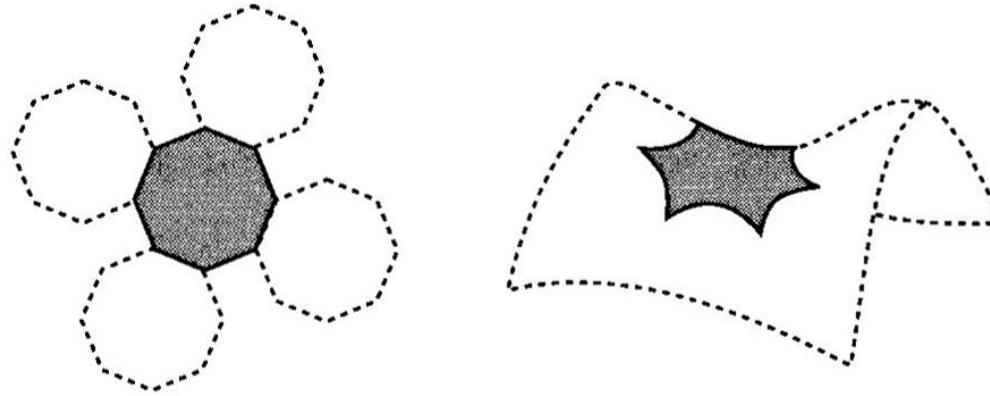


Figure 13.10. Paving the hyperbolic plane with octagons. It is impossible to pave the Euclidean plane with octagons, which implies that the double torus is not a Euclidean surface. On the other hand, the hyperbolic plane can be paved by octagons cut from the hollow of a saddle. The hyperbolic plane is thus the universal covering space for the double torus. The eight corners of the octagon must all be identified as a single point; this is the reason why one must use a negatively curved octagon with angles of 45 degrees ($8 \times 45 = 360$), in place of a flat octagon, whose angles are each 135 degrees.

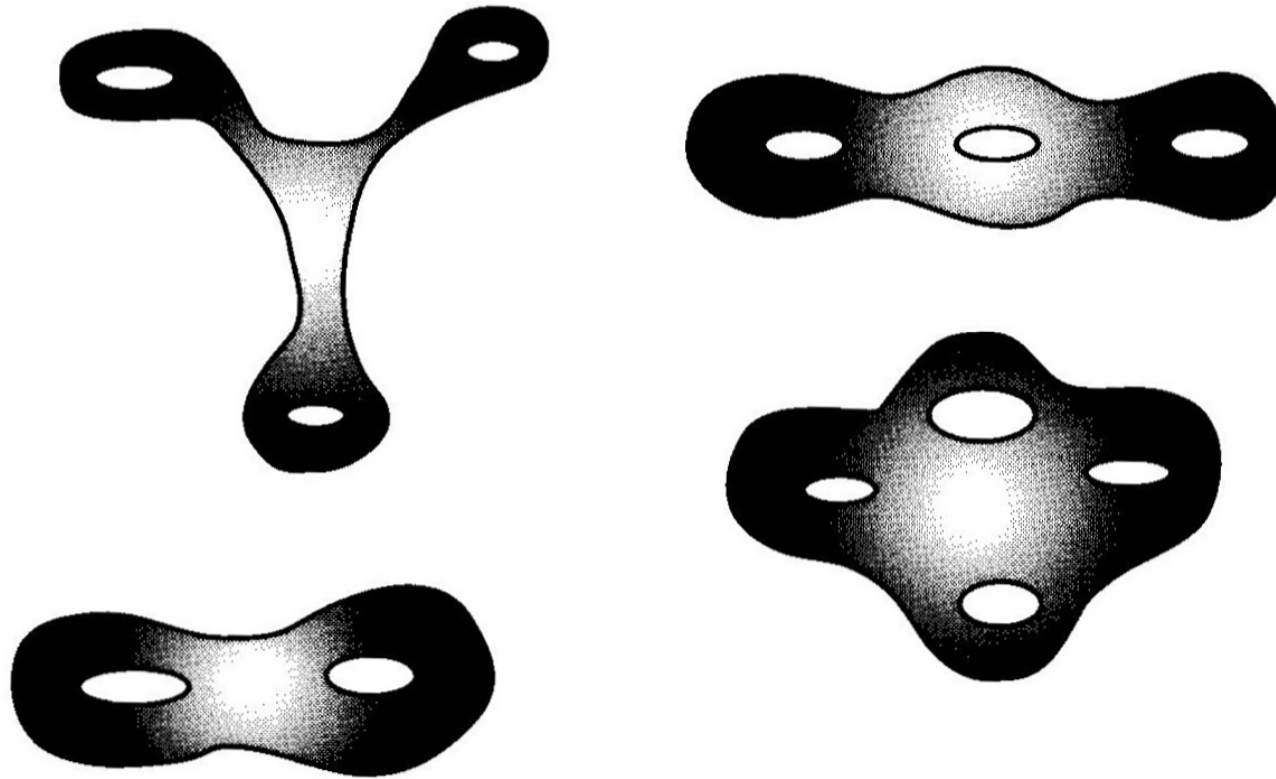


Figure 13.13. Hyperbolic pretzels. All closed surfaces having more than one hole are spaces of negative curvature, equipped with a hyperbolic geometry.

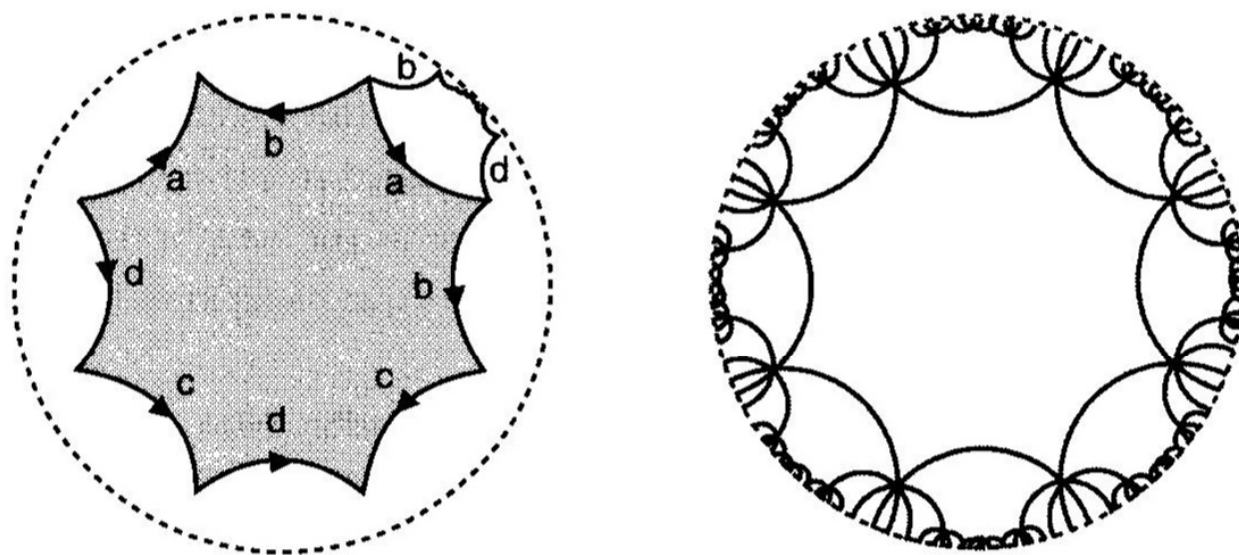


Figure 13.12. Poincaré's representation of the hyperbolic plane. By acting with the holonomies on each point of the fundamental octagon, and repeating the process again and again, one creates a paving of the hyperbolic plane by regular and identical octagons. Poincaré demonstrated that the hyperbolic plane, normally infinite, could be represented entirely within the interior of a disk, whose edge represents infinity. Poincaré's model deforms distances and shapes, which explains why the octagons seem irregular and increasingly tiny as we approach the boundary of the disk. All of the lines in the figure represent straight lines of the hyperbolic plane, and meet the boundary at a right angle.

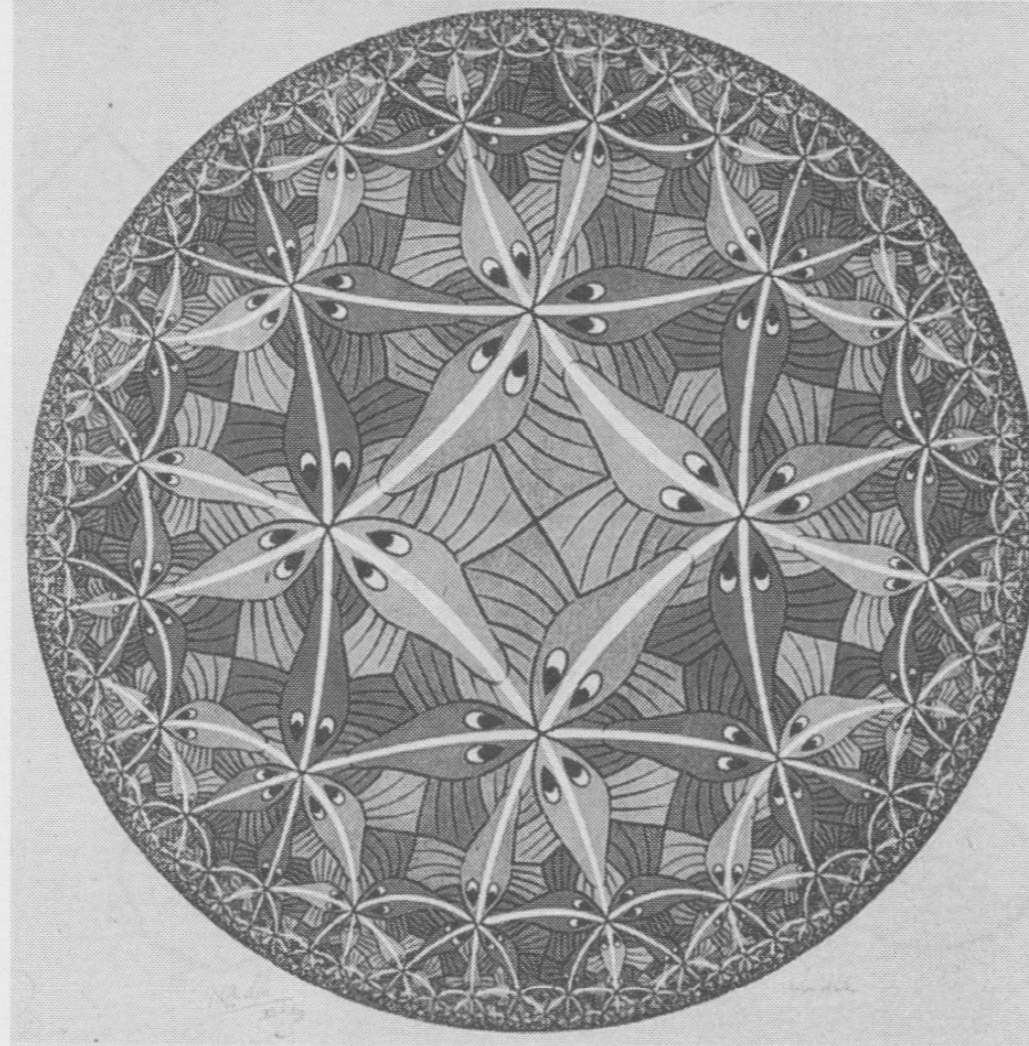


Figure 13.11. Circle Limit. In this 1959 woodcutting, Escher has used the representation given by Poincaré to pave the hyperbolic plane using fish. (See Plate II. M. C. Escher's "Circle Limit III," © 2007 The M.C. Escher Company-Holland. All rights reserved. www.mcescher.com.)

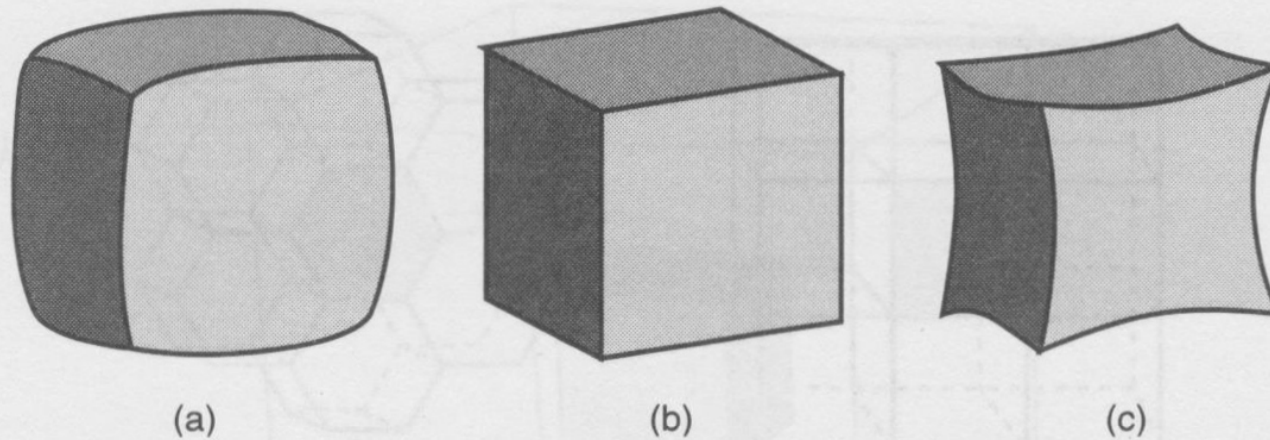


Figure 14.5. Spherical, Euclidean, and hyperbolic polyhedra. In a spherical space (a), polyhedra have larger angles than in Euclidean space (b), while in hyperbolic space (c), polyhedra have smaller angles.

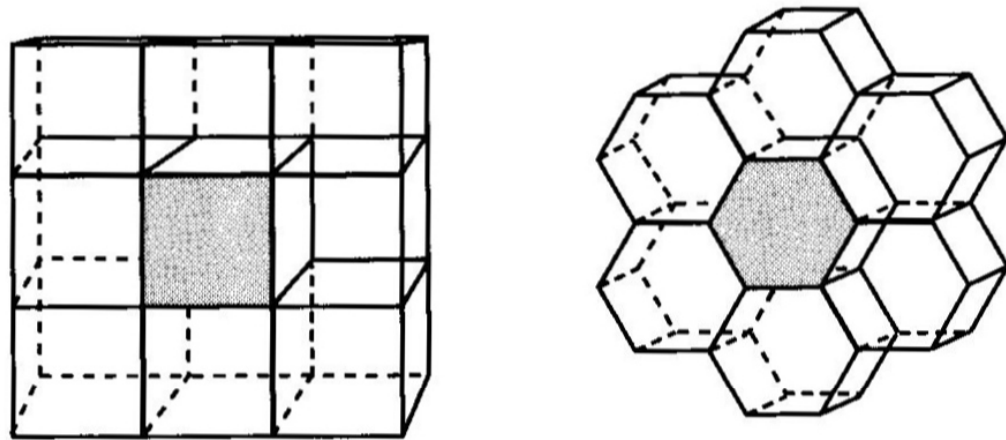


Figure 14.3. Two tilings of Euclidean space. In three dimensions, ordinary Euclidean space can be regularly “paved” by rectangular parallelepipeds or by hexagonal prisms.

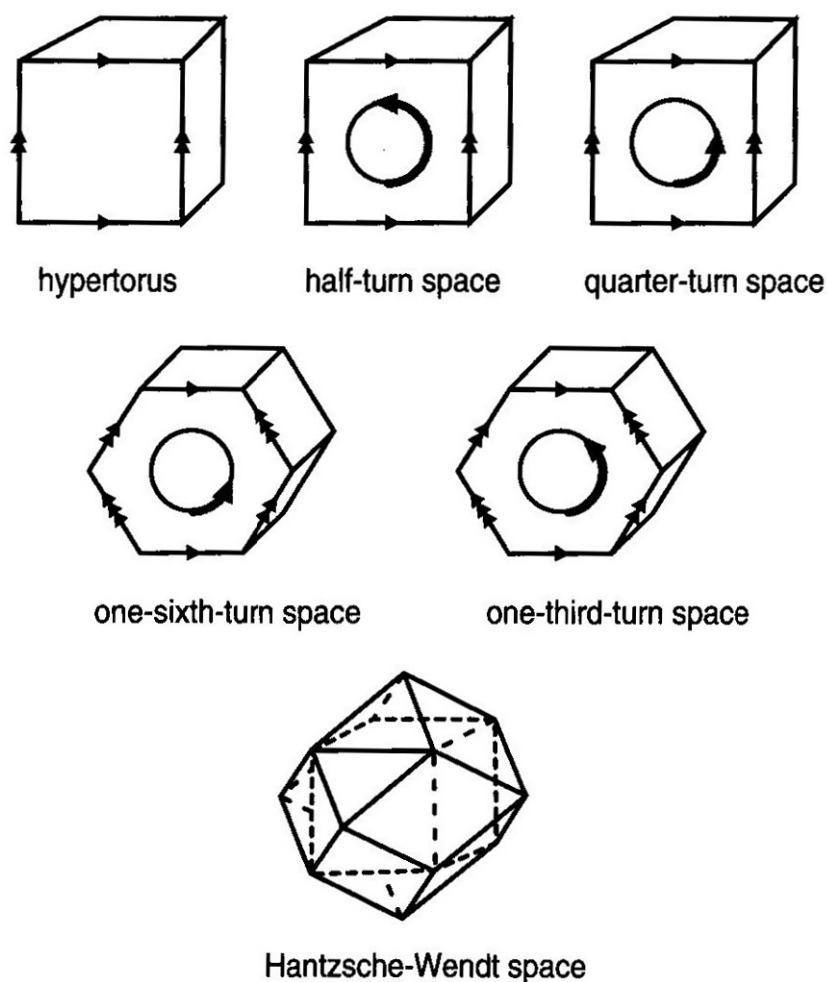


Figure 14.4. Six small Euclidean spaces. By properly identifying the opposing faces of a parallelepiped or a hexagonal prism, one obtains six finite and orientable Euclidean spaces. For the simplest of them, the hypertorus T^3 , the identification is made through simple translations. For the others, one of the faces from the pair (here the front and back faces) is turned by $1/2$, $1/4$, $1/6$, or $1/3$ of a full rotation before being glued. The sixth space, discovered by Hantzsche and Wendt in 1935, has a more complicated structure based on the rhombic dodecahedron.

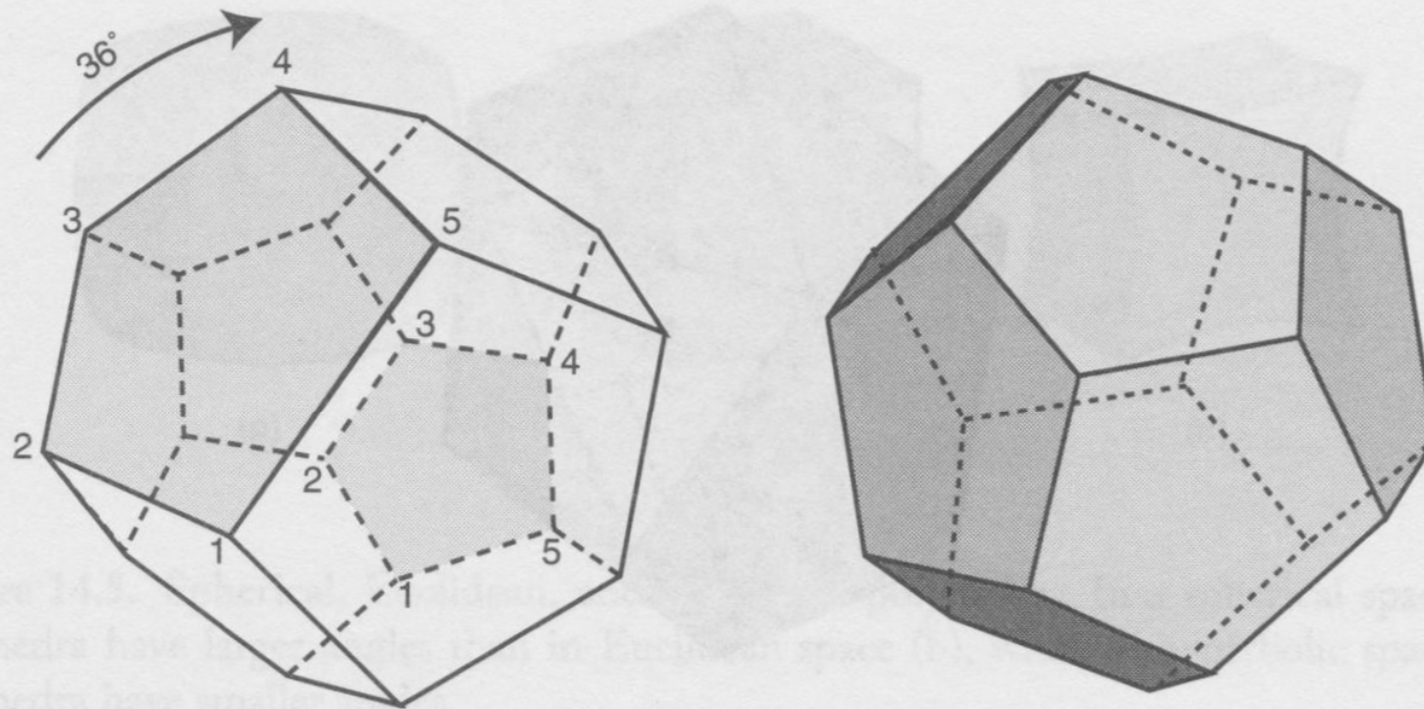


Figure 14.7. Poincaré's spherical space. If each face of a dodecahedron is glued to its opposing face after undergoing a 36° rotation (one tenth of a complete rotation), the resulting space is Poincaré's spherical space, a multiply connected variant of the hypersphere, whose volume is now 120 times smaller. However, this gluing can only be completed if one uses a positively curved dodecahedron, with edge angles of 120° rather than $\sim 117^\circ$, as in Euclidean space.

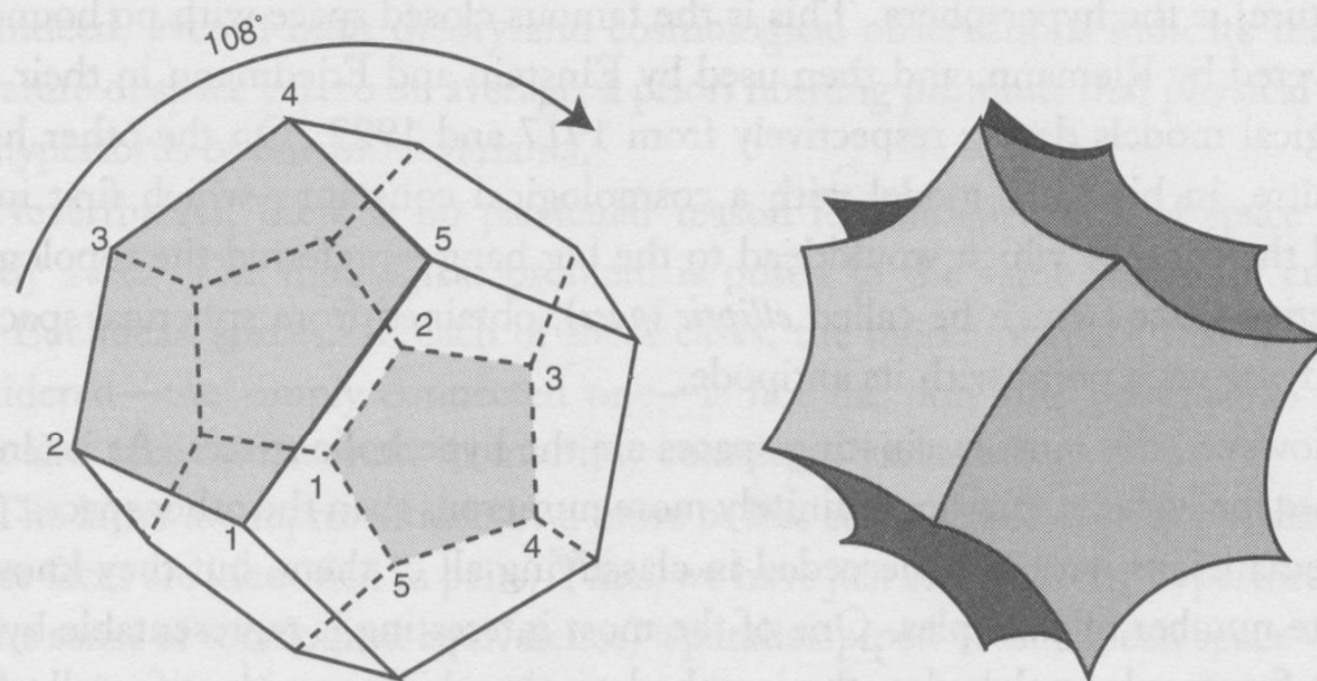


Figure 14.8. The Seifert-Weber hyperbolic space. If each face of a dodecahedron (at left) is glued to its opposite face after being rotated by 108° (three tenths of a complete rotation), the resulting space is the Seifert-Weber hyperbolic space, a multiply connected variant of the hyperboloid H^3 , with finite volume. As for the octagon in Figure 13.10, the gluing can only be accomplished if one uses a negatively curved dodecahedron, with angles shrunk to 72° (on right).

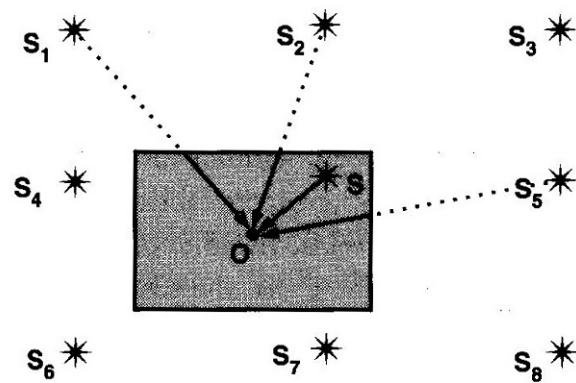
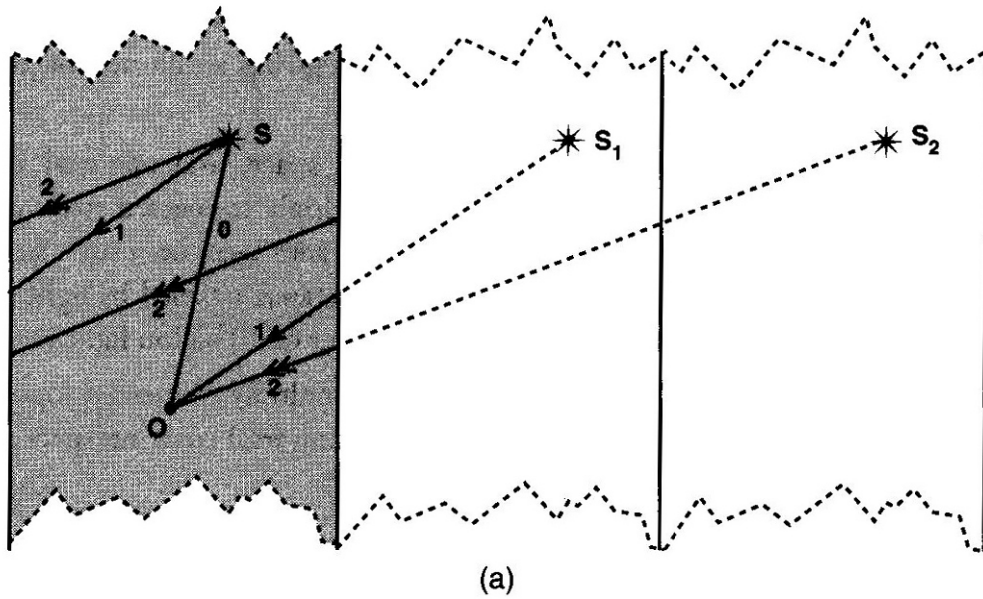


Figure 16.1. The illusion of the universal covering. (a) In the case of the cylinder, real space is the interior of the gray band, whose edges are identified. Light rays emitted by the source S arrive at the observer O along several paths, corresponding to the differing numbers of loops they have made around the cylinder. The observer O , therefore, has the illusion of seeing several distinct sources (S , S_1 , S_2 , etc.) aligned within a fictional space made up from the juxtaposition of endlessly repeating bands—the universal covering space of the cylinder. (b) In the case of the torus, the real space is the interior of the gray rectangle, whose opposite edges are identified. The observer O sees rays of light from the source S coming from several directions. He has the illusion of seeing distinct sources (S_1 , S_2 , S_3 , etc.) distributed along a regular canvas that covers an infinite plane.

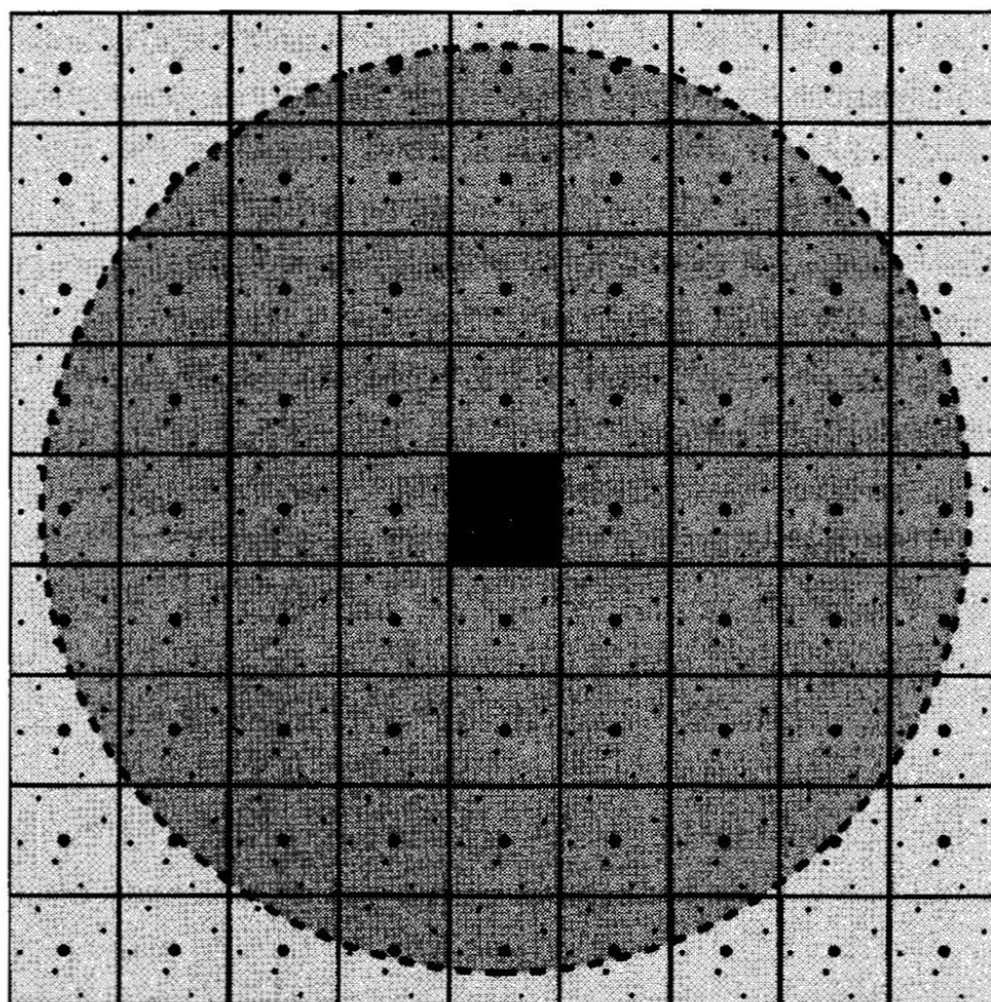


Figure 16.2. The illusion of the infinite. In practice, space-time horizons bound the view of the observer, because of which the observer only perceives a limited portion of the universal covering space. In this toric space (center square) the observable universe is found within a circular horizon (dotted line), containing only a finite number of replicas of the fundamental cell.

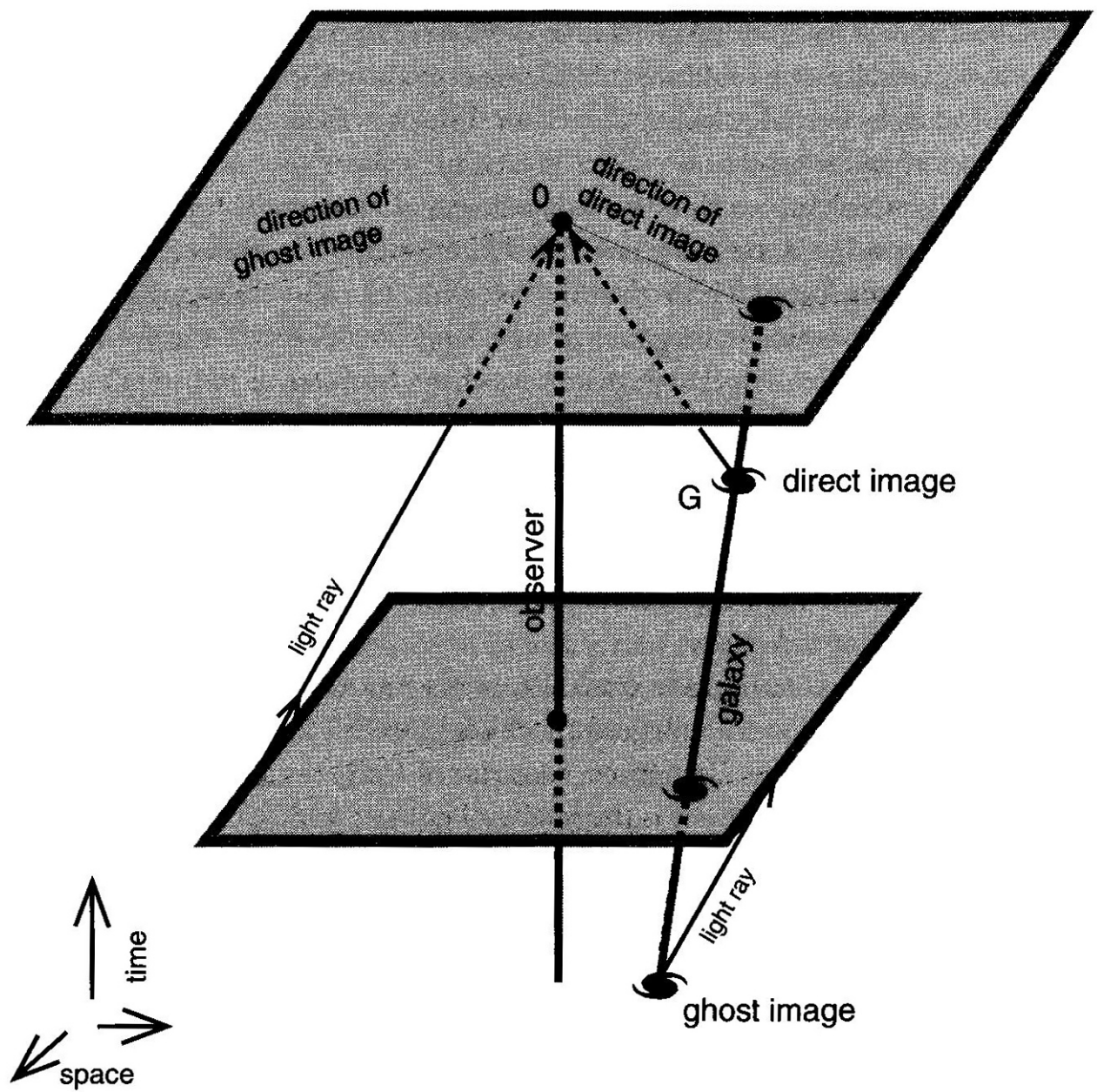


Figure 16.3. The ghosts belong to the past. Light rays come from the past. In this space-time representation of an expanding toric universe, rays of light received at the same time by an observer O come from the same galaxy G , but they have been emitted at different epochs. The “original” image of G is the most recent; the ghost images are necessarily older.

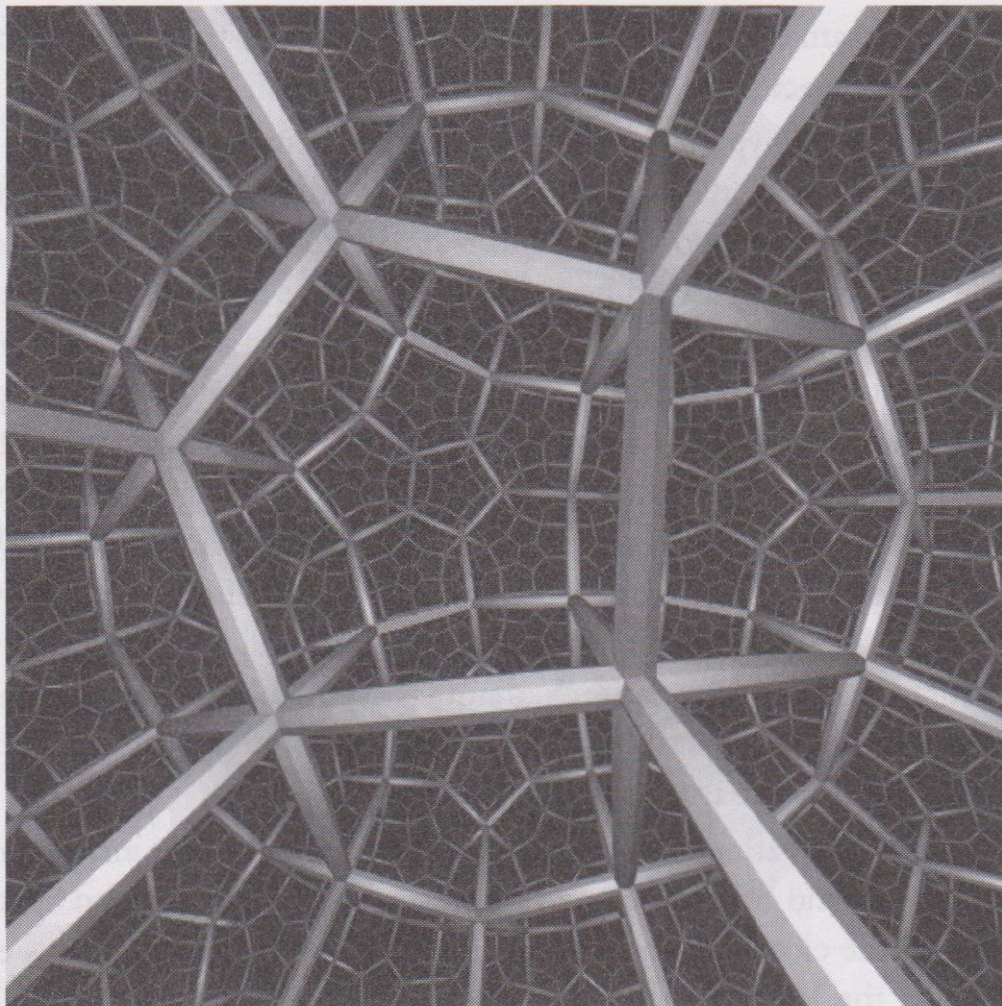


Figure 17.1. A cosmic hyperbolic crystal. A wraparound universe has a remarkable topology that allows an identification of physical space with a polyhedron, whose multiplied image makes up the world of appearances. To represent the structure of apparent space reduces to representing its “crystalline” structure, of which each cell is a reproduction of the fundamental polyhedron. Here we illustrate the apparent structure that would be offered by the closed hyperbolic Seifert-Weber space (see Figure 14.8). Viewed from the interior, one would have the impression of living in a cellular space, paved out to infinity by dodecahedra deformed by optical illusions. (See Plate III. Image from the film *Not Knot*, ©A K Peters, Ltd.)

In conclusion, the multiple images of a given object appear to us in different directions, with different brightnesses, from different orientations and at different epochs of its history. Therefore, they do not resemble each other. This is why it is difficult to know if the Universe is wrapped through direct identification: a great part of that which we take for original galaxies could well be nothing but ghost replicas of a limited number of real galaxies, replicas that it would be impossible, in the absence of a precise stamp, to recognize as such.

Researchers have, nevertheless, made the attempt. Boudewijn Roukema and Alastair Edge have put forth the hypothesis that the strong luminosity in the domain of x-rays emitted by certain galaxy clusters could constitute a distinctive stamp. This actually comes from gas internal to the cluster, in which the galaxies bathe, which is heated to several million degrees and emits this high-energy radiation, which is detectable at a very great distance. These x-ray clusters are, moreover, dynamically stable; they may therefore prove to be more efficient than other localized sources of radiation at displaying the topology. In 1997, Roukema and Edge suggested that the Coma cluster, cluster RXJ 1347.5-1145, and cluster CL 09104 + 4109, viewed at differing spectral redshifts, but all three of which exhibit strong x-ray luminosity, could be the ghost images of a single, unique cluster in a non-orientable hypertoric topology (a sort of three-dimensional Klein bottle). Their hypothesis is difficult to refute, but the chances that this is a pure coincidence are too great for such detection of ghosts to be credible.

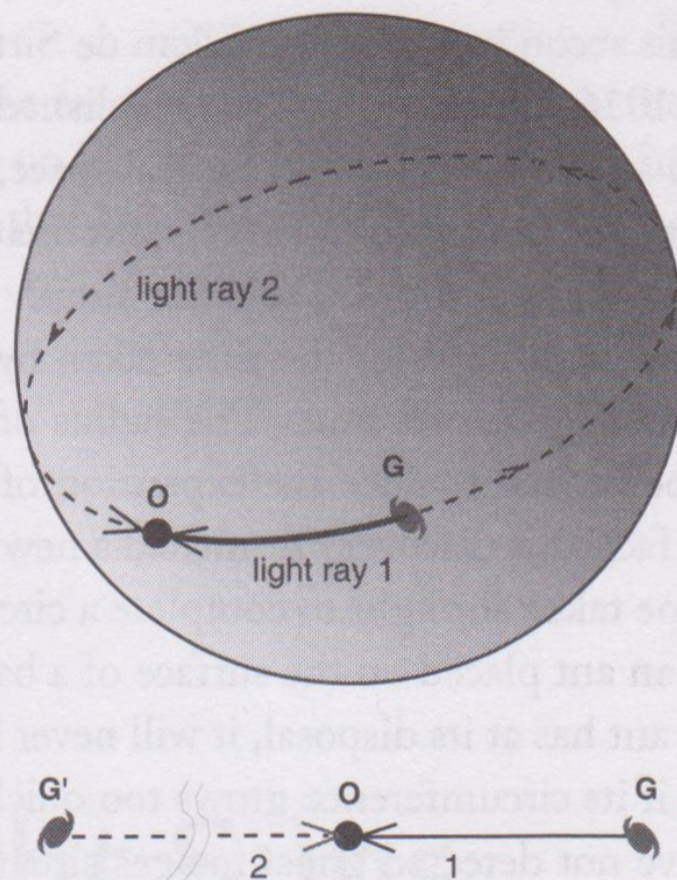


Figure 19.1. The circumnavigation of space. In a hyperspherical space, an observer O should in principle see light rays emitted by a galaxy G coming from two opposite directions. However, if the expansion of the universe is rapid enough, light ray 2 will never succeed in making it around space, because of which the observer will never see the phantom image G' .

In 1913, in the framework of a controversy on the reality of curved space, Barrett Frankland remarked that, in a spherical space, each star would show its front and back sides in two opposite directions of the sky. Thus, one should see two Suns: the ordinary Sun, meaning the image of the star such as it was 500 seconds ago (the time taken by light to travel the 150 million kilometers that separate us from it), and the anti-Sun, situated at the antipode of the celestial sphere and showing it such as it was a long time ago (the time taken for light to travel the circumference of the Universe). From this, Frankland concluded that there should no longer be any darkness on Earth, since the anti-Sun would shine during the night! Consequently, according to him, the hypothesis was false, and Frankland rejected the existence of a spherical space.

Zwicky, which contains 9,730 clusters of all types. All have a redshift smaller than 0.2 and are therefore found at a distance of less than 2.5 billion light years. At this distance, the rich clusters are necessarily original; in fact the closest clusters that are observed are also poorer, and since the natural tendency of clusters is to enrich themselves over the course of their evolution, the poor clusters cannot represent the rich clusters in a later state.

The constraint on the size of space imposed by these various observations is $L > 2.5$ billion light years. There is still a lot of room up to the distance of the cosmological horizon. The radius of the latter depends on the value of the cosmological parameters. For example, in a Euclidean Universe (with zero spatial curvature) without cosmological constant, it is 18 billion light years, while in a Universe with the same curvature but with a cosmological constant of 0.7, it reaches 50 billion light years. The hypothesis of a wraparound space that is smaller than observed space therefore remains perfectly viable.

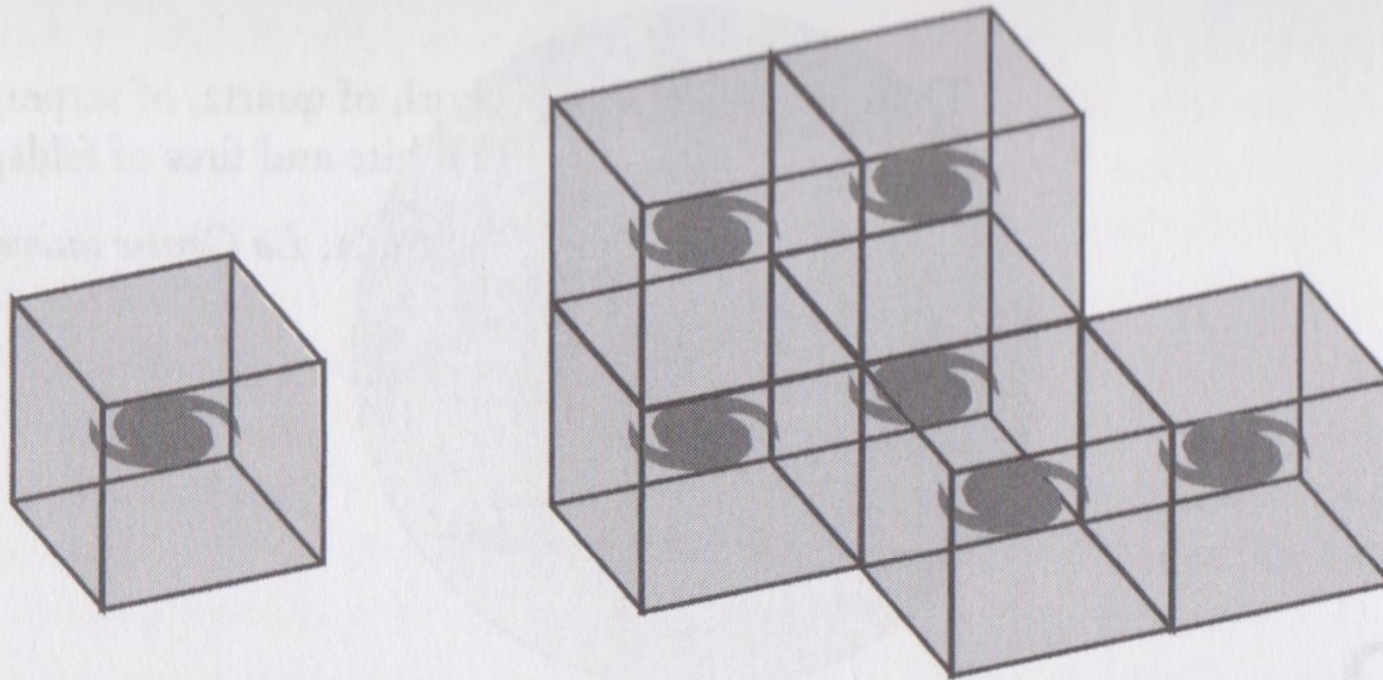


Figure 20.1. Multiple milky ways. In 1900, the astronomer Karl Schwarzschild already had imagined that our galaxy, the Milky Way, could repeat itself endlessly within a regular cubic framework, thus giving the illusion of a space that is vaster than it really is.

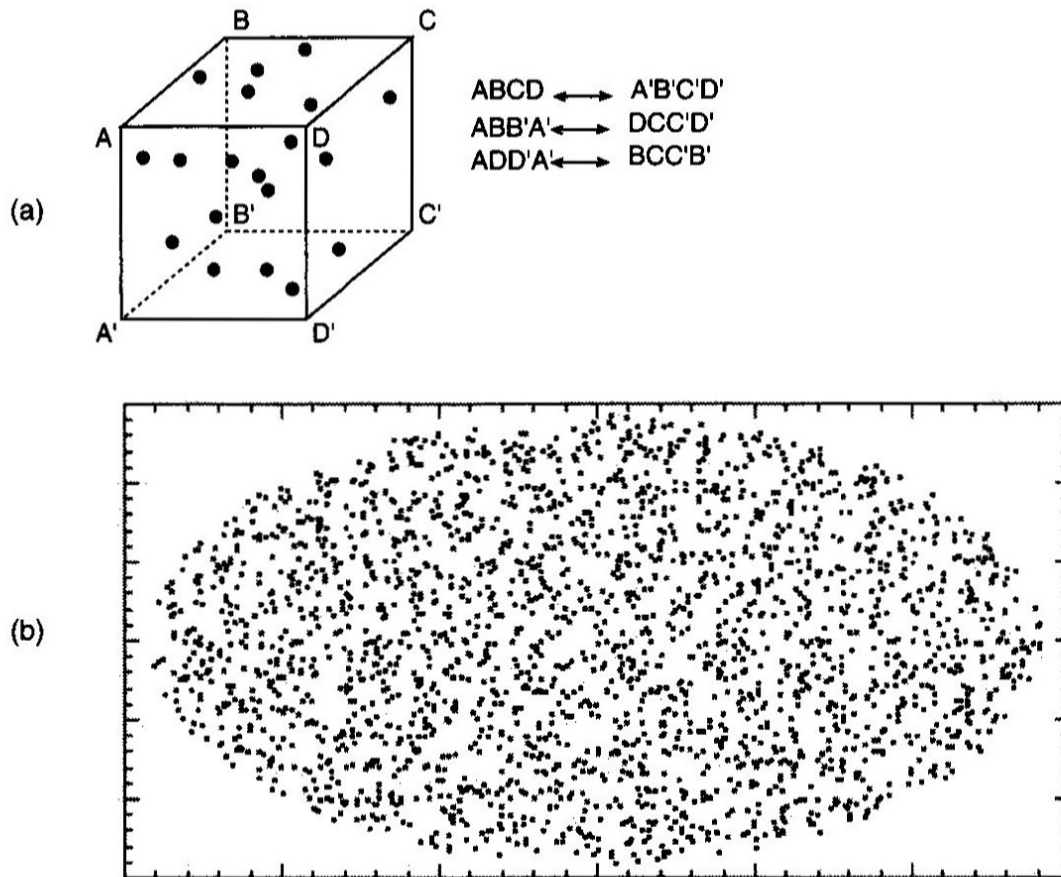


Figure 20.2. A cosmic unit cell. (a) The space here is a hypertorus, represented by the interior of a cube with edges that are five billion light-years in length, whose opposite faces are identified. Twenty galaxies are distributed randomly within the space. (b) This shows a numerical simulation of the appearance of the sky after accounting for the effect of topological mirages. Each real galaxy leads to about 50 ghost images spread throughout the celestial vault. Among the hundreds of visible images, it is impossible to separate the real images from the ghosts.

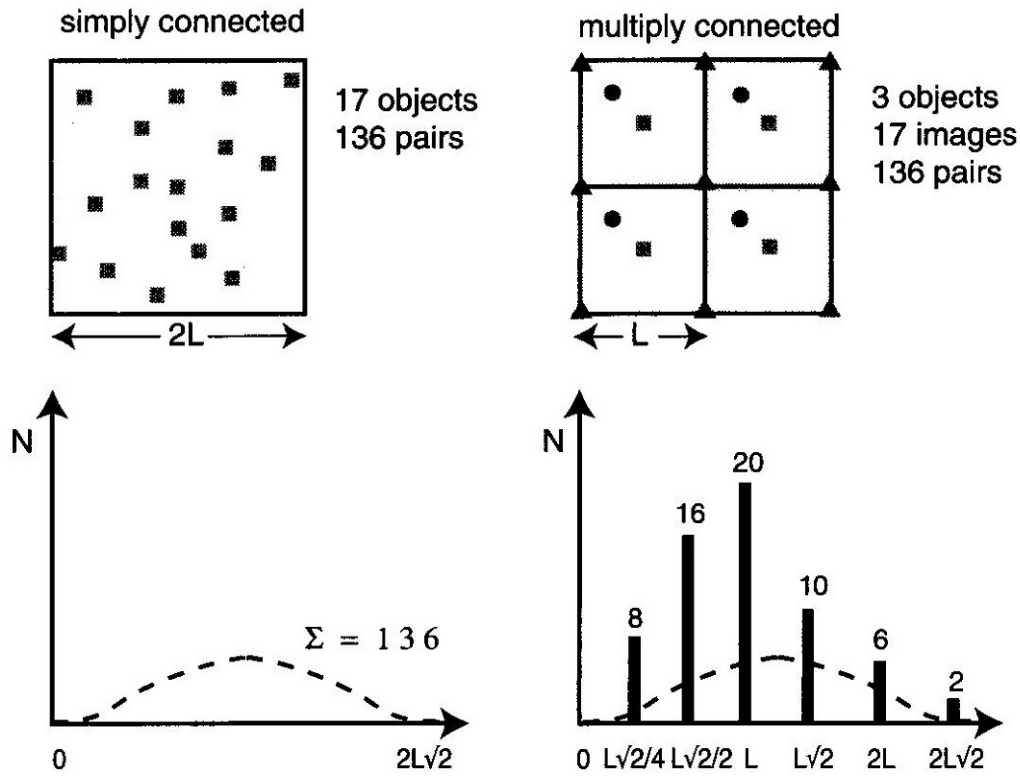


Figure 20.3. The histogram method. At left, a piece of simply connected space with surface area $4L^2$ contains 17 distinct objects, leading to 136 possible pairs. Below, the histogram of separations is a bell curve spread between zero (the minimum distance) and $2L\sqrt{2}$ (the maximum distance, equal to the diagonal of the square). The integral is equal to 136. At right, a piece of space with the same surface area of $4L^2$ is in fact a mosaic formed from four repetitions of a small toric space of length L , containing only three original objects (a square, a point, and a triangle aligned along half of a diagonal). The mosaic contains 17 topological images, leading to 136 pairs. This time, however, the distribution is no longer arbitrary, as the histogram below it shows: 8 pairs are separated by a distance of $L\sqrt{2}$, 16 pairs by $4L\sqrt{2}/2$, 20 pairs by L , etc. The accumulation of pairs having the same distance therefore gives rise to spikes.

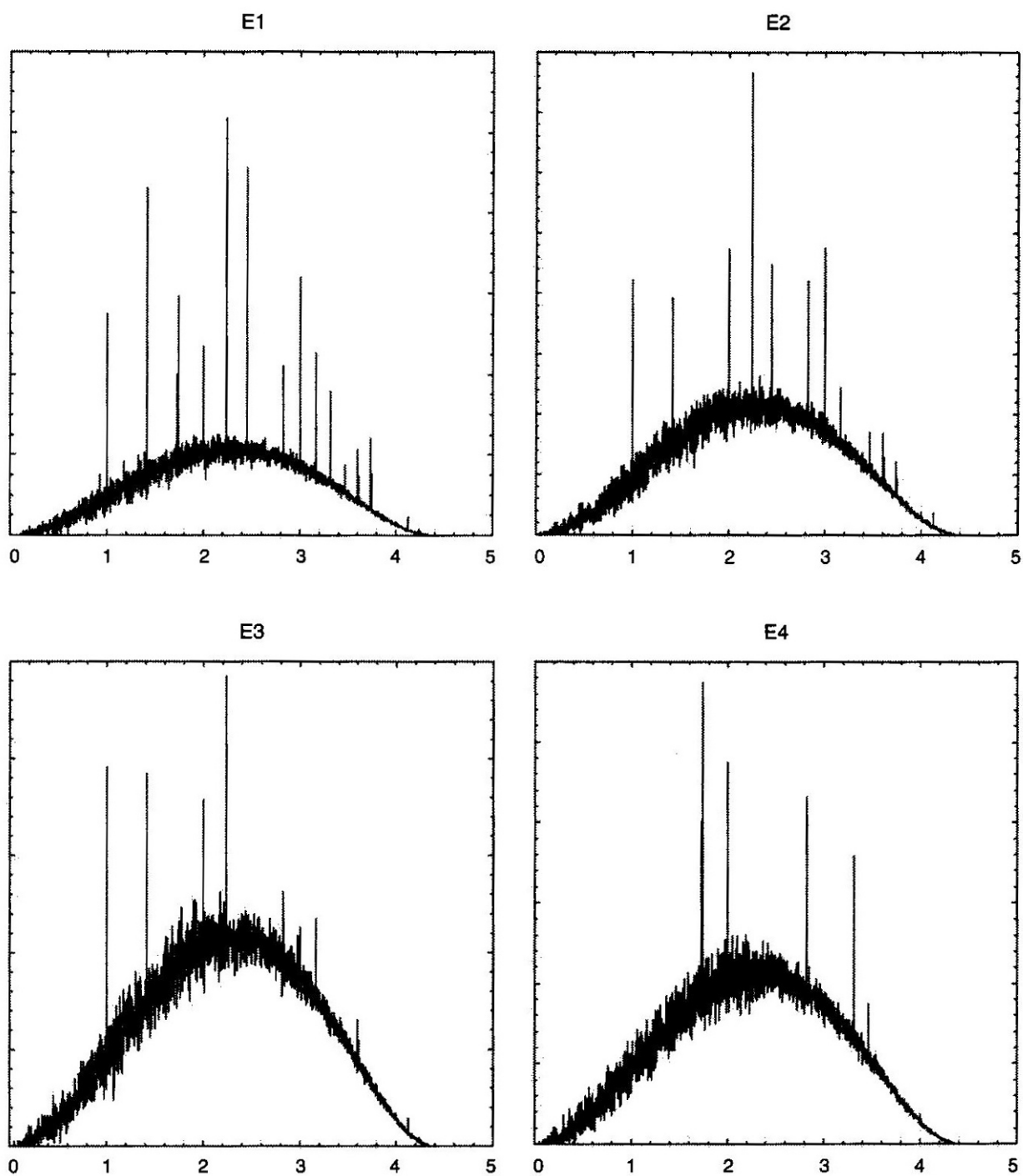


Figure 20.4. The histogram method. These numerical simulations apply the method of histograms for pairwise separations to four Euclidean wraparound spaces. The presence of peaks signals a multiply connected topology, their positions reflect the size of the fundamental polyhedron, and their relative heights characterize the holonomy group.

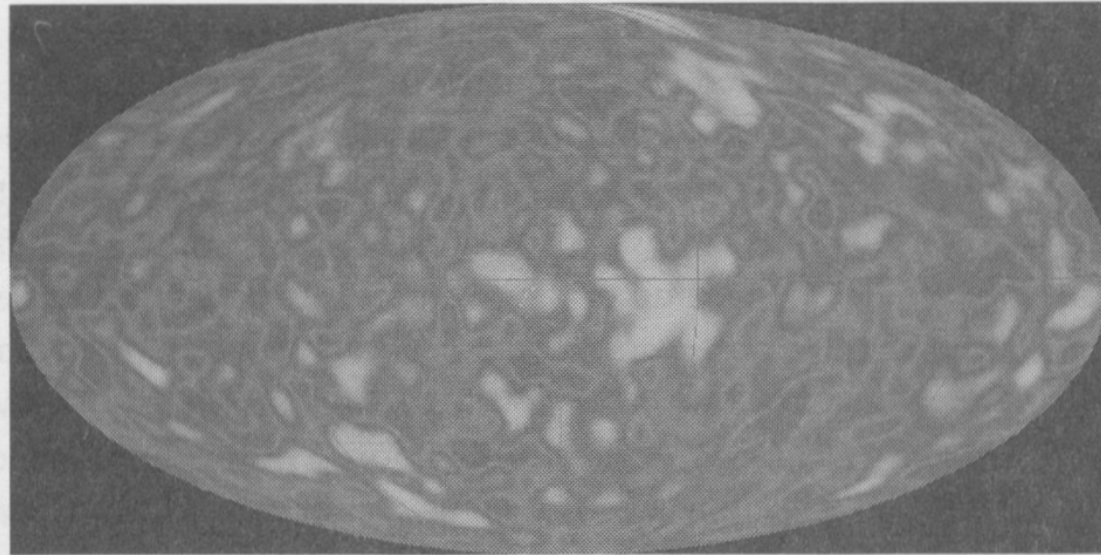


Figure 21.2. Fluctuations of the fossil radiation. Emitted at a temperature of 3,000 degrees Celsius, the radiation of the cosmological background reaches us at a temperature one thousand times smaller, in the microwave scale. This microwave map of the sky, taken in 1992 by the astronomical satellite COBE, represents the state of the Universe 14 billion years ago, at the epoch when there was only a homogeneous plasma, with the exception of minuscule variations in the temperature, encoded here by different colors. The maximal difference between the warmest points (dark red) and the coolest points (light blue) is no more than one hundred thousandth of a degree. (See Plate VI. Image from NASA COBE.)

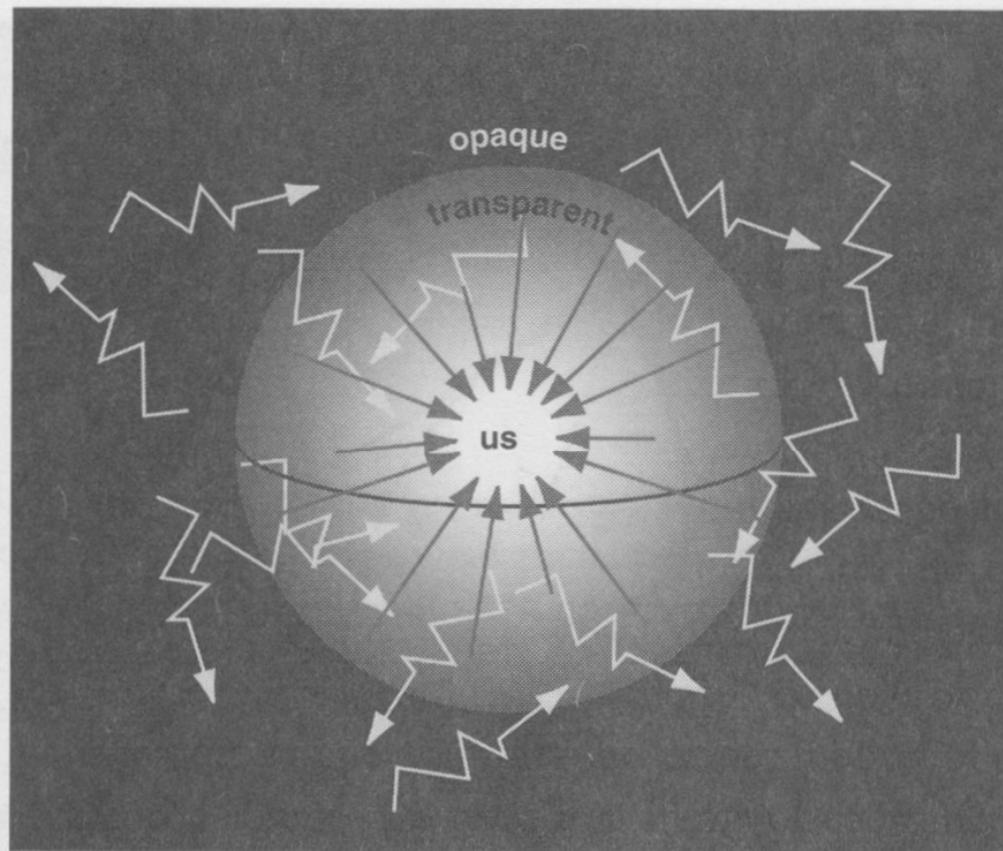


Figure 21.1. The surface of last scattering. The fossil radiation fills space-time, but the photons whose energy we can measure are those that arrive here and now. They all began their voyage at the same instant of cosmic history, around 14 billion years ago, and at the same distance from us: at the surface of last scattering, which marks the transition between an opaque universe and a transparent universe.

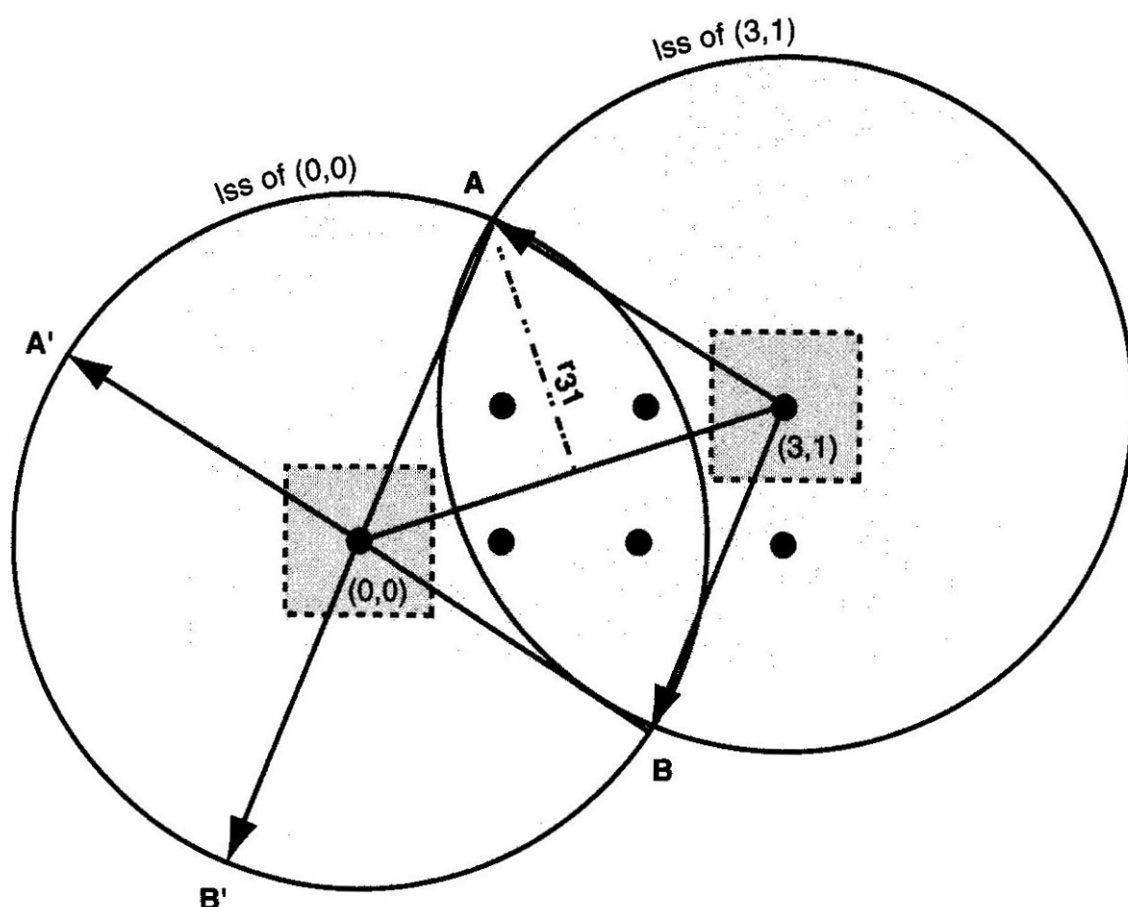


Figure 21.3. Principle of the method of matched circles. The method of matched circles is illustrated here in a wraparound space of two dimensions (a torus). The fundamental polyhedron is a square (with a dotted outline); all of the dark gray points are copies of the same observer. The two large circles (which are normally spheres in a three-dimensional space) represent the last scattering surfaces (lss) centered on two copies of the same observer. One is in position (0, 0); its copy is in position (3,1) in the universal covering space. The intersection of the circles is made up of the two points A and B (in three dimensions, this intersection is a circle). The observers (0,0) and (3, 1), who see the two points (A, B) from two opposite directions, are equivalent to a unique observer at (0, 0) who sees two identical pairs (A, B) and (A', B') in different directions. In three dimensions, the pairs of points (A, B) and (A', B') become a pair of identical circles, whose radius r_{31} depends on the size of the fundamental polyhedron and the topology.

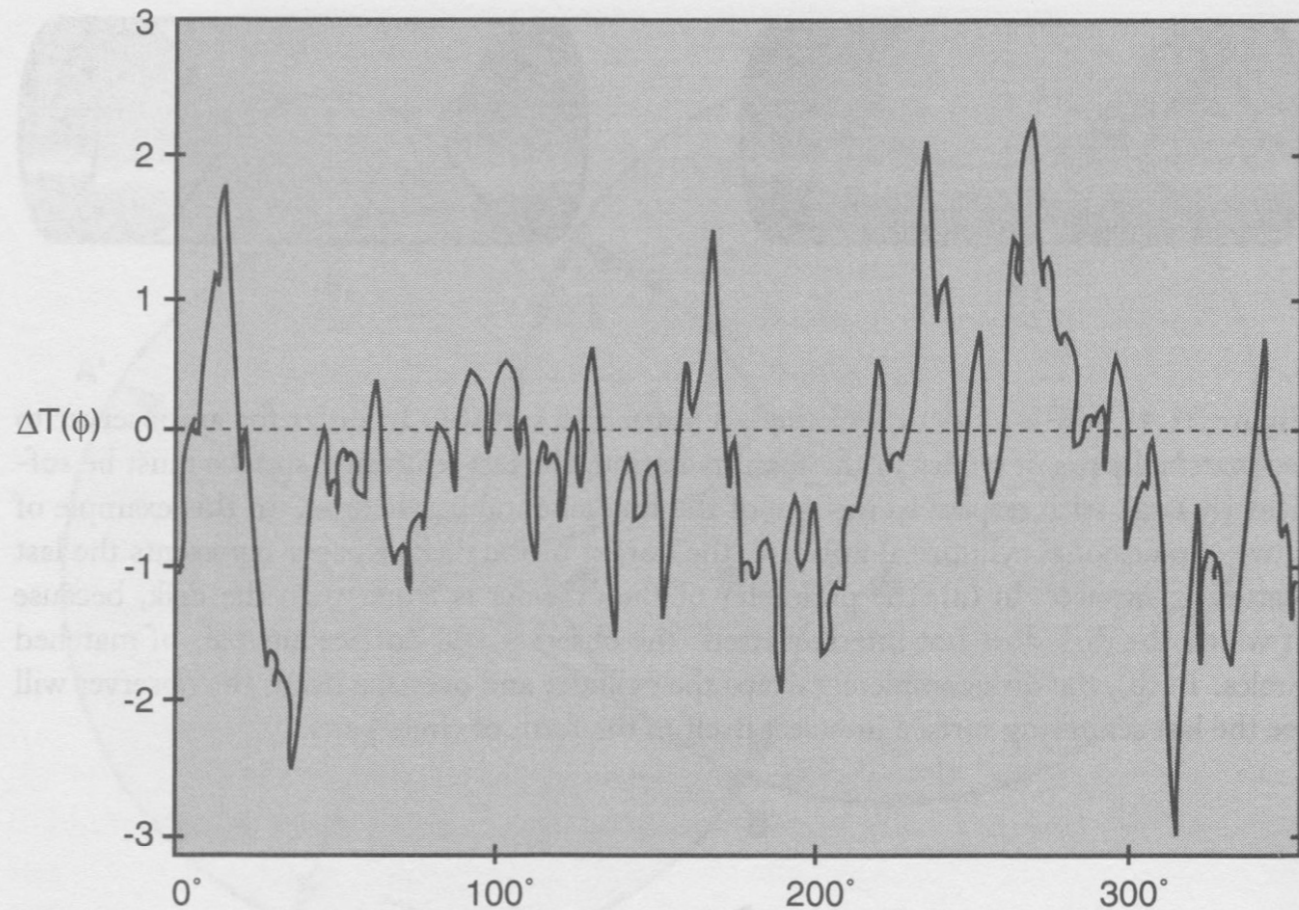


Figure 21.6. Temperature curve of a cosmic circle. Along an arbitrary circle traced on the last scattering surface (represented on the x -axis by an angle varying from 0° to 360°), the temperature (the y -axis) varies by a few millionths of a degree around an average value. Although the average temperature is the same for all circles (this is the cosmological black-body temperature), the temperature curve varies in a specific way along each circle. If two circles having the same temperature curve are viewed in two different directions of the sky, they indicate a pair of matched circles within a wraparound space.

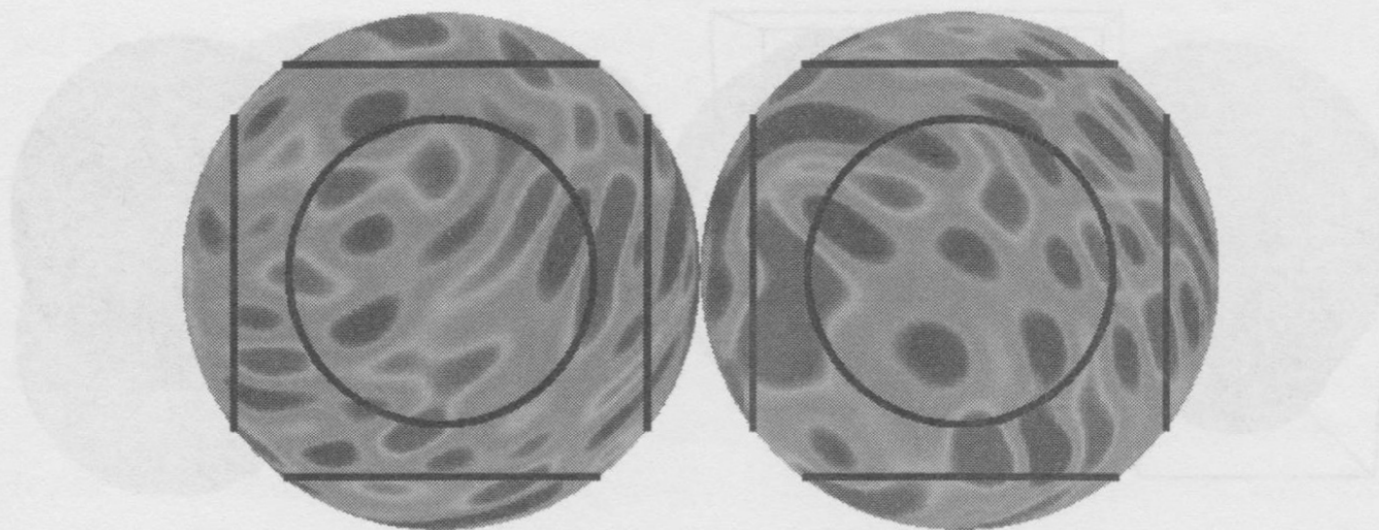


Figure 21.7. Identification of circles by their temperature curves. The WMAP and Planck satellites will furnish data on the microwave background in the form of a very precise map of the temperatures in the sky's background—represented here in the form of a western hemisphere and an eastern hemisphere. The warmest regions are in red, the coolest in blue (the maximum distance between these two extremes is no greater than 0.00001 degrees). If space is a hypertorus, and if the last scattering surface is large enough to completely wrap it in every direction, one will observe pairs of matched circles (in black). The matched circles are characterized by equal temperatures at corresponding points. Follow with your left index finger the central circle of the western hemisphere in a clockwise direction, starting from twelve o'clock. Simultaneously, follow with your right index finger the central circle of the eastern hemisphere, now turning in a counter-clockwise direction. You will pass through the same temperatures at corresponding points. The search for matched circles in the real Universe will be complicated by various sources of noise, which have been omitted in this simple illustration. (See Plate VII. Image courtesy of Jeffrey Weeks.)

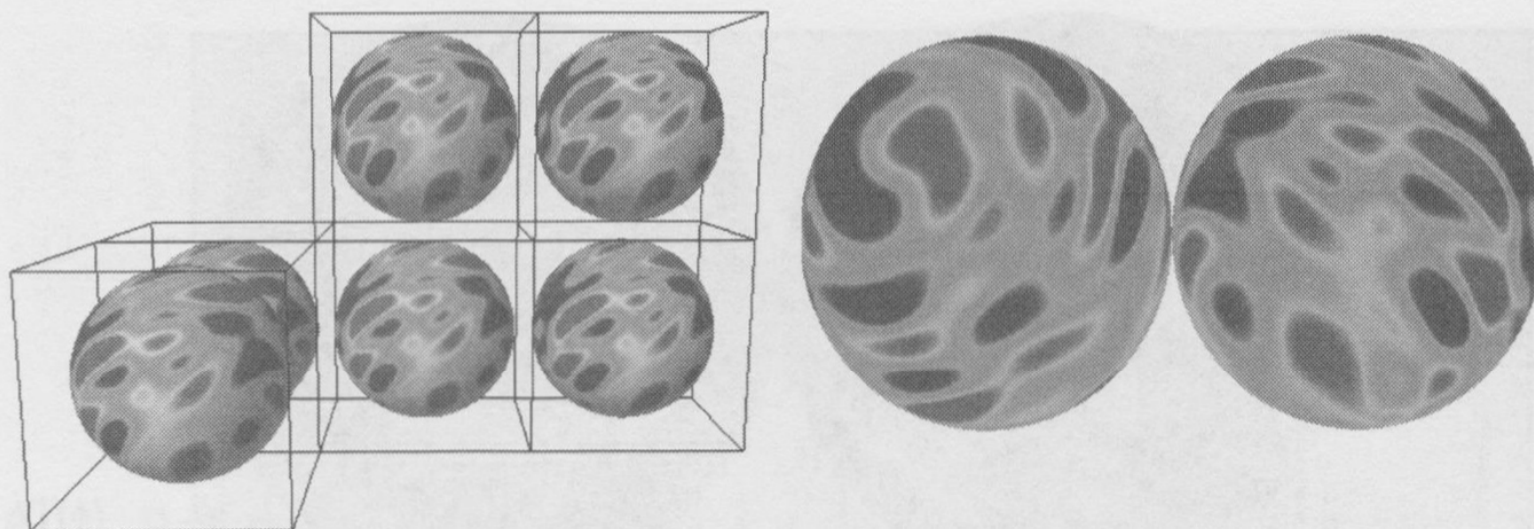


Figure 21.8. A large hypertoric universe. The space is a hypertorus, but its fundamental polyhedron is larger than the last scattering surface (network at left). The last scattering surface does not intersect itself, and no circle pairs appear in maps of the fossil radiation (shown at right in the form of two hemispheres). (See Plate VIII. Image courtesy of Jeffrey Weeks.)

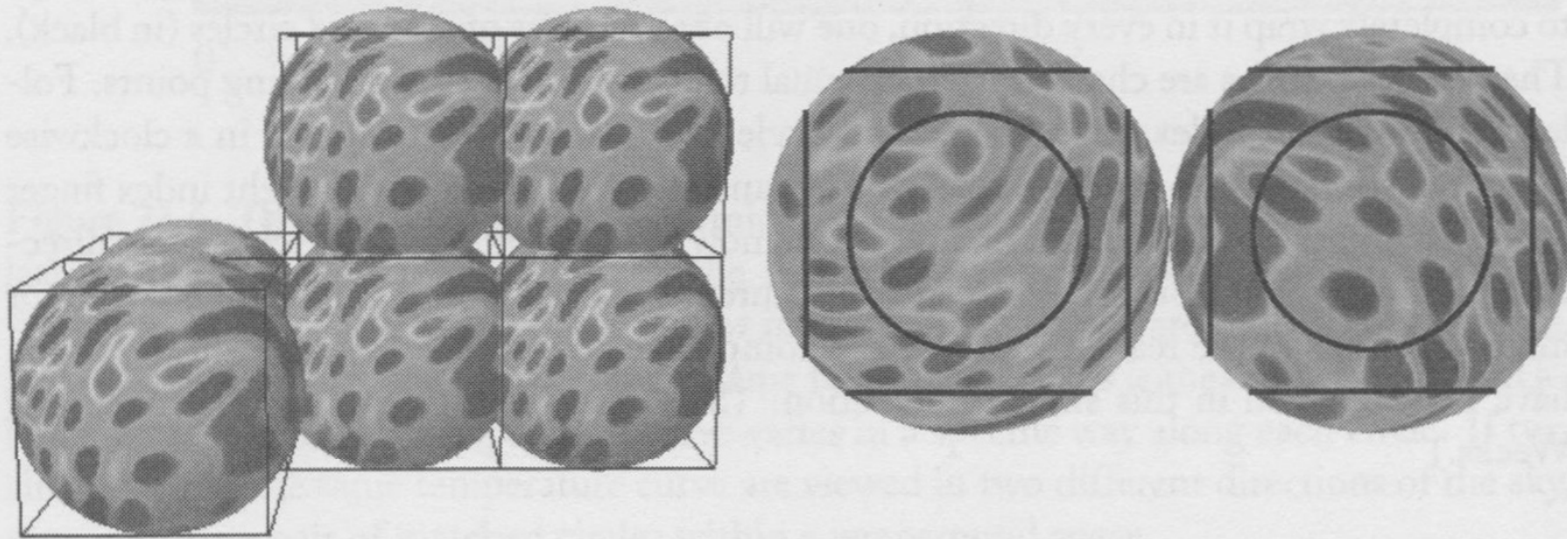


Figure 21.9. An averagely small hypertoric universe. The space is a hypertorus, but its fundamental polyhedron is slightly smaller than the last scattering surface (network at left). This is just large enough to cover space in every direction and intersect itself: one will observe three pairs of matched circles (in black in the maps on the right). Each circle corresponds with the one directly opposite to it. (See Plate IX. Image courtesy of Jeffrey Weeks.)

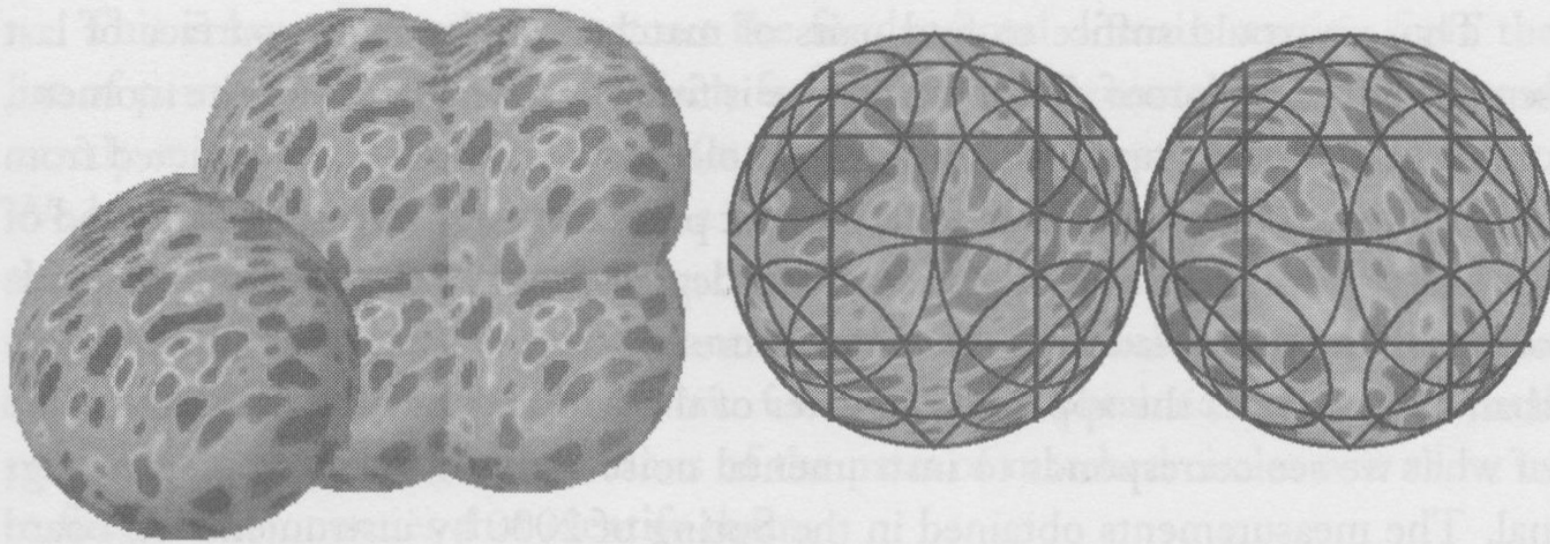


Figure 21.10. A very small hypertoric universe. The space is still a hypertorus, but the fundamental polyhedron is much smaller than the last scattering surface (network at left). This overlaps itself numerous times, and one will observe a great number of pairs of matched circles (in black in the maps on the right). (See Plate X. Image courtesy of Jeffrey Weeks.)

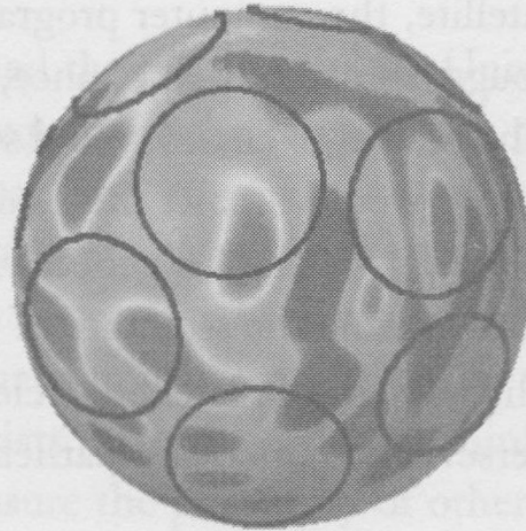


Figure 21.11. Matched circles in an icosahedral universe. If the matched circles form an icosahedral pattern, the Universe itself must be represented by an icosahedral space like that of Figure 14.6 (the Best space). For a more complicated topology, the circular patterns will be more complicated as well. In any case, the relative disposition of pairs of circles will reveal the topology of the Universe. (See Plate XI. Image courtesy of Jeffrey Weeks.)

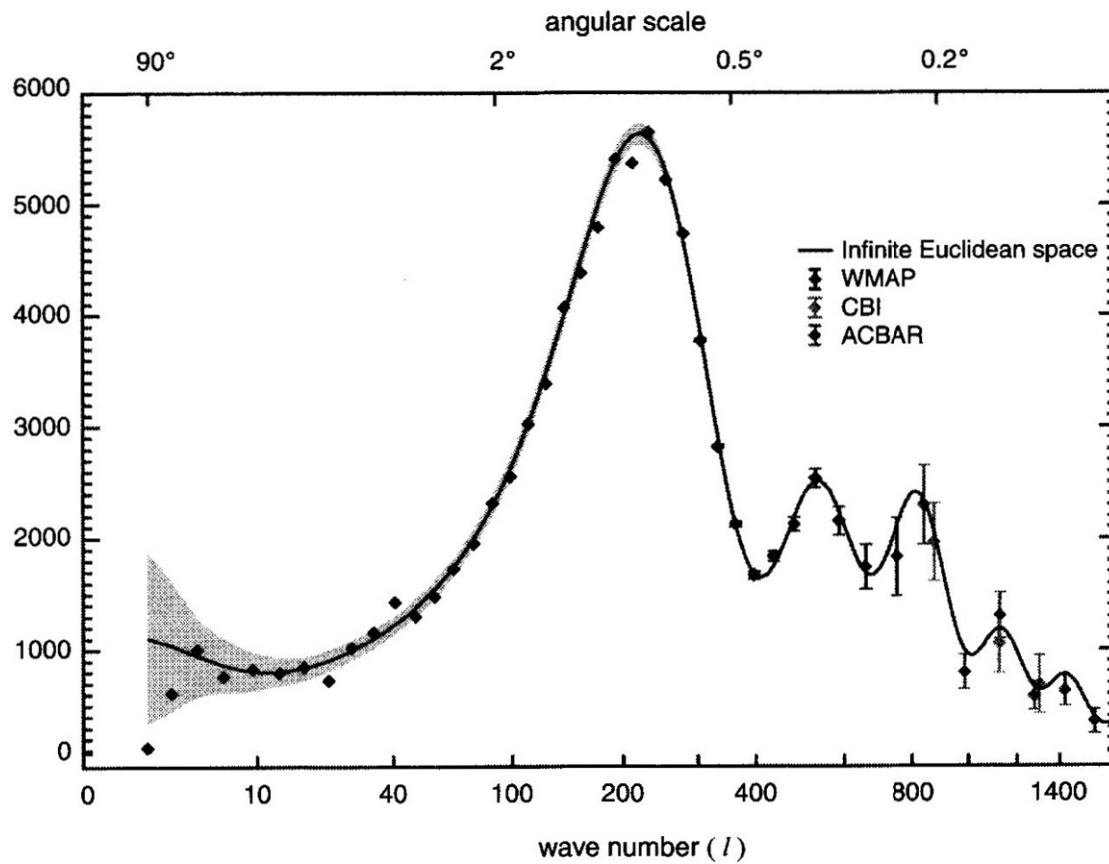


Figure 45.4. Power spectrum of the cosmic microwave background. The data from the WMAP satellite (black diamonds) have improved the precision of the spectrum far beyond that obtained by earlier measurements. The diagram reflects the small differences in temperature in the fossil radiation. The spectrum exhibits a series of peaks corresponding to small angular separations (or, equivalently, large wave numbers l). The main peak corresponds to the angular size of the most frequent lumps from Figure 45.3. The position and amplitude of this peak in particular allow one to constrain the curvature of space. At larger angular separations, this structure disappears and the data predicted by the standard model are expected to follow a plateau. However, the WMAP measurements fall well below the plateau in the range of the lowest wave numbers, named the quadrupole ($l = 2$) and the octopole ($l = 3$). The infinite, Euclidean cosmological model (giving the theoretical curve) cannot explain this, while well-proportioned finite models for the universe with multiply-connected topologies explain it very well. (Image from NASA/WMAP Science Team.)